Spatial Versus Temporal Stability Issues in Image Processing Neuro Chips

Takashi Matsumoto, *Fellow, IEEE,* Haruo Kobayashi, *Member, IEEE,* and Yoshio Togawa

***Abstract*—A typical image processing neuro chip consists of a regular array of very simple cell circuits. When it is implemented by a CMOS process, two stability issues naturally arise:**

- **i) Parasitic capacitors of MOS transistors induce the *temporal* dynamics. Since a processed image is given as the stable limit point of the temporal dynamics, a temporally unstable chip is unusable.**
- **ii) Because of the array structure, the node voltage distribution induces the *spatial* dynamics, and it could behave in a wild manner, e.g., oscillatory, which is highly undesirable for image processing purposes, even if the trajectory of the temporal dynamics converges to a stable limit point.**

The main contributions of this paper are (i) a clarification of the spatial stability issue; (ii) explicit *if and only if* conditions for the temporal and the spatial stability in terms of circuit parameters; (iii) a rigorous explanation of the fact that even though the spatial stability is stronger than the temporal stability, the set of parameter values for which the two stability issues disagree is of (Lebesgue) *measure zero*; and (iv) theoretical estimates on the processing speed.

I. Introduction

A. Motivation

THIS study has been motivated by the temporal versus spatial stability issues of an image smoothing neuro chip [1]. The function of the chip is to smooth a two-dimensional image in an extremely fast manner. It consists of the 45×40 hexagonal array of very simple "cell" circuits, described by Fig. 1. An image is projected onto the chip through a lens (Fig. 2) and the photo sensor represented by the current source in Fig. 1 inputs the signal to the processing circuit. The output (smoothed) image is represented as the node voltage distribution of the array. With an appropriate choice of $g_0 > 0$, $g_1 > 0$, and $g_2 < 0$, the chip performs a *regularization* with *second-order* smoothness constraint and closely approximates the Gaussian convolver, which is known to have an optimal S/N as a preprocessor for edge detection [2], [3]. (APPENDIX IV explains why a regularization with second-order smoothness constraint demands negative conductance.) Conductance g_0 is designed to be variable in order to control the width of the Gaussian-like kernel. In engineering terms, this is a noncausal infinite impulse response (IIR) realization of a Gaussian-like convolver instead of a finite impulse response (FIR) realization, and this structure accomplishes high-speed processing while maintaining simplicity. The reader is referred to [1] for responses actually measured from the chip.

Since the *negative conductance* $g_2 < 0$ is involved, two stability issues naturally arise:

(i) Because the chip is fabricated by a CMOS process, parasitic capacitors induce the dynamics with respect to time. This raises the *temporal stability* issue of whether the network converges to a stable equilibrium point.

(ii) Because a processed (smoothed) image is given as the node voltage distribution of the array, the *spatial stability* issue also arises even if the temporal dynamics does converge to a stable equilibrium point. In other words, the node voltage distribution may behave in a wild manner, e.g., oscillatory.

In discussing relationships between the temporal and the spatial stability issues, several precautions need to be taken. In particular, it is important to realize that while the temporal dynamics is *causal*, i.e., $t \geq 0$, the spatial "dynamics" (a precise definition will be given later) is *noncausal*. Namely the spatial dynamics can go into the negative direction as well as the positive direction. Furthermore, the spatial dynamics is not an initial value problem but rather a *boundary value problem* which gives rise to several delicate issues.

Our earlier numerical experiments on these issues were rather intriguing. The results suggested that the network is temporally stable "if and only if" it is spatially stable. Fig. 3 shows spatial impulse responses at different sets of parameter values. For the sake of simplicity, the network is of a linear array instead of a two-dimensional array. The network has 61 nodes and the impulse is injected at the center node. Fig. 3(a) suggests that the network can be used for image smoothing because the response to an impulse is "bell-shaped." In fact, the Gaussian-like convolver chip [1] corresponds to Fig. 3(a) where g_0 is variable. Fig. 3(b) indicates that it can enhance contrast of an input image after smoothing because it inhibits the "surround" responses in addition to smoothing. Fig. 4 shows the corresponding temporal step responses of the center node. For simplicity, the only parasitic capacitors taken into account are those from each node to the ground. The responses shown in parts (a) and (b) of Fig. 4 are temporally stable while part (c) is not. Fig. 3(c) is spatially unstable because the response does not decay, which is highly undesirable for image

Manuscript received January 15, 1991; revised October 9, 1991. This work was supported by the Japanese Ministry of Education, the Ogasawara Foundation, the Casio Foundation, and the Science and Engineering Laboratory and Tokutei-Kadai of Waseda University.

T. Matsumoto is with the Department of Electrical Engineering, Waseda University, Tokyo 169 Japan.

H. Kobayashi is with Yokogawa Electric Corporation, Tokyo 180, Japan.

Y. Togawa is with the Department of Information Science, Science University of Tokyo, Tokyo, Japan.

IEEE Log Number 9105239.

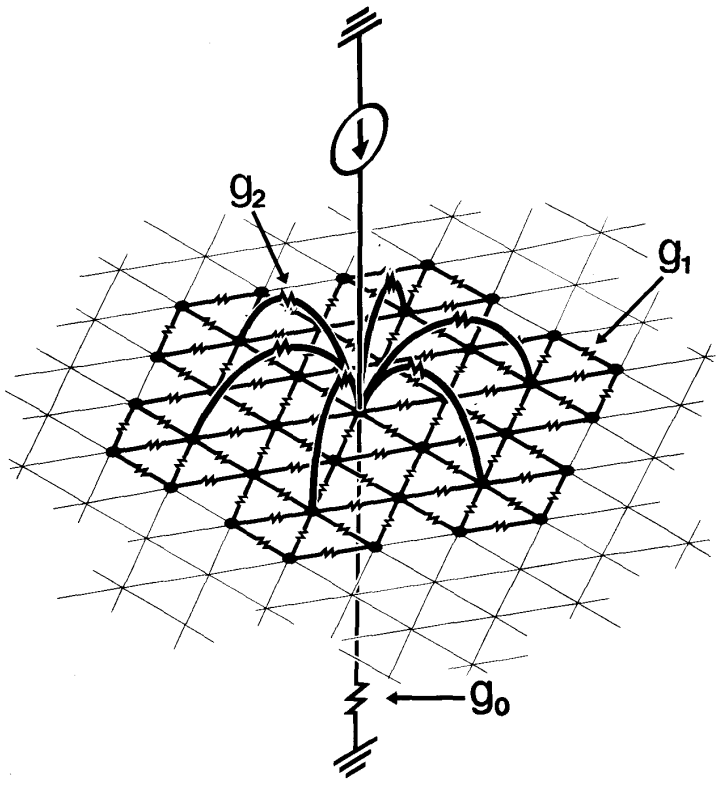

Fig. 1. The image smoothing neurochip. Only one "unit" is shown.

processing purposes. (A precise definition of spatial stability will be given later.) All of our earlier numerical experiments, including those shown in Fig. 3 and Fig. 4, suggested the equivalence of the two stability conditions. However there are no *a priori* reasons for them to be equivalent. As will be shown rigorously, the two stability conditions are *not* equivalent. The spatial stability condition is *stronger* than the temporal stability condition. Nevertheless, the set of parameter values (g_0, g_1, g_2) for which the two stability conditions disagree turns out to be a (Lebesgue) *measure zero* subset, which explains why our numerical experiments suggested equivalence between the two conditions. (A measure zero subset is difficult to "hit"). We will prove, in a very general setting, that the network is temporally stable if and only if it is *spatially regular,* a new concept which is weaker than the spatial stability, and it amounts to a decomposability of eigenvalues of a matrix describing the spatial dynamics. Explicit analytic conditions will be given for the temporal as well as the spatial stabilities in a general setting. Also given is an estimate on the speed of temporal responses of the networks.

Since our results are proved in a general setting, they can be applied to other neural networks of a similar nature, e.g. oriented receptive field filters [4] and Gabor filters [5], which we intend to pursue in our future projects. The results in this paper, however, are only for linear array cases. Extensions to two-dimensional array cases are nontrivial and are left for a future paper.

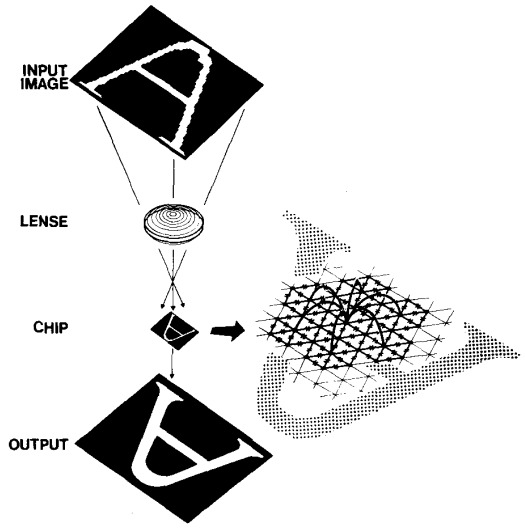

Fig. 2. A schematic diagram.

B. Related Works

A serious stability analysis is performed in [6] for lateral inhibition networks that are present, at least partly, in most

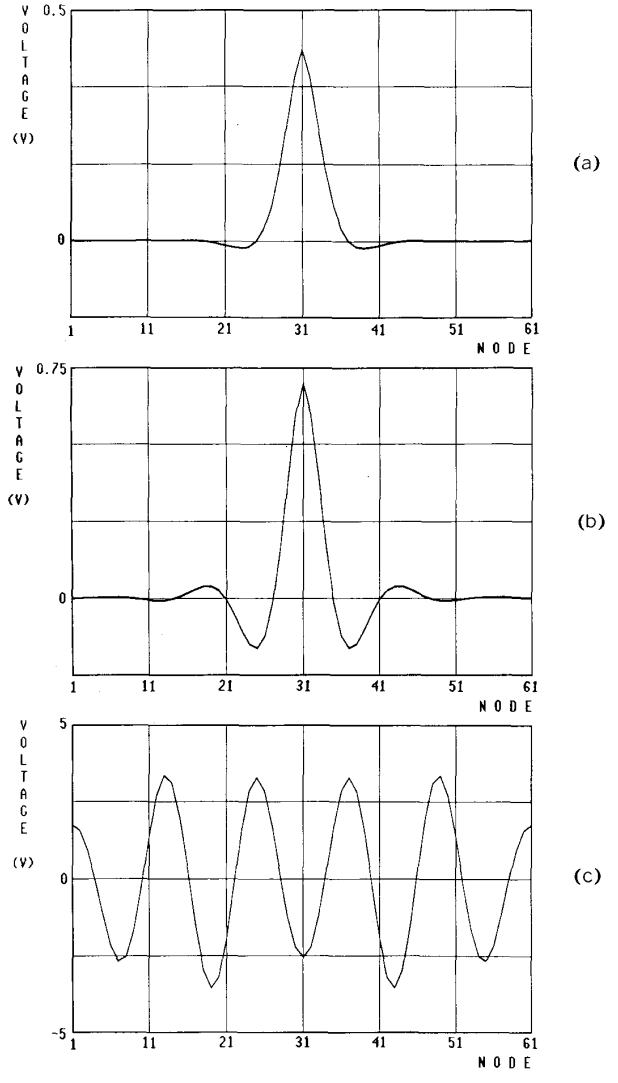

Fig. 3. Spatial impulse responses with $n = 61$, $m = 2$, $1/g_0 = 200$ kΩ, $1/g_1 = 5$ kΩ, $u_{31} = 10$ μA, $u_k = 0$ for $k \neq 31$. (a) $1/g_2 = -20$ kΩ; stable. (b) $1/g_2 = -18$ kΩ; stable. (c) $1/g_2 = -17$ kΩ; unstable.

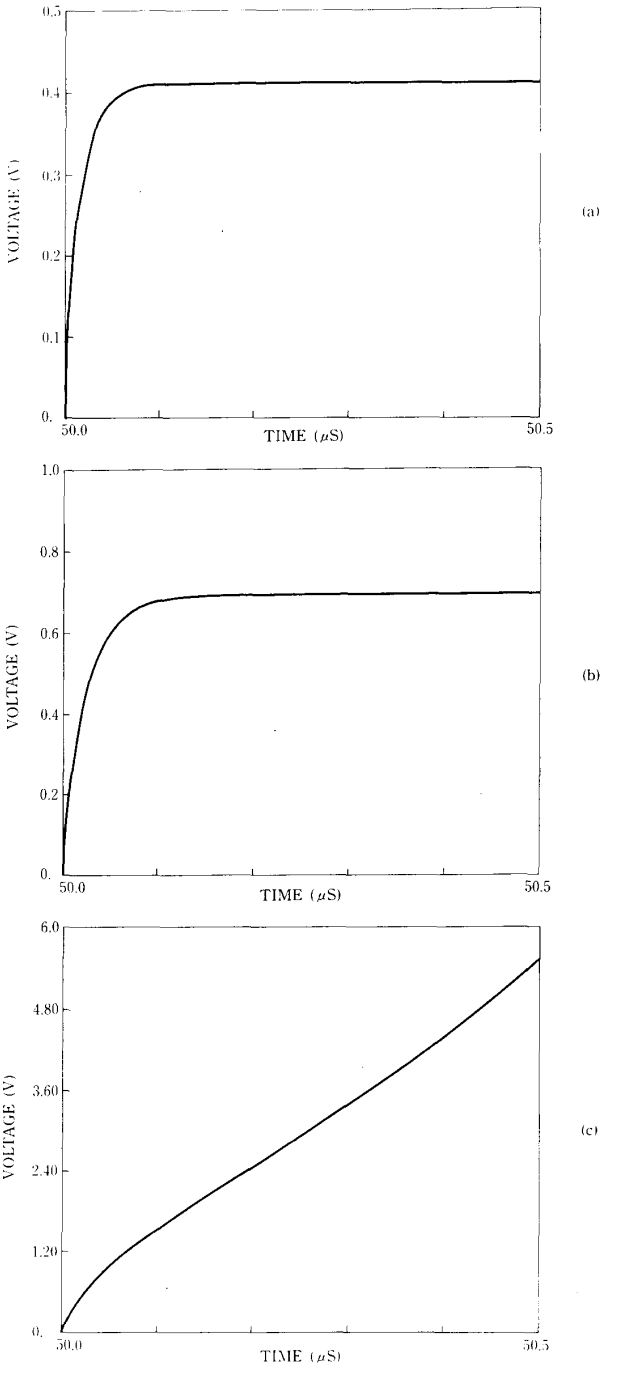

Fig. 4. Temporal step responses of the center node $v_{31}(t)$ with $n = 61$, $m = 2$, $1/g_0 = 200$ kΩ, $1/g_1 = 5$ kΩ, $c_0 = 0.1$ pF,

$$u_{31}(t) = \begin{cases} 0 & t < 50\ \mu s \\ 10\ \mu A & t \geq 50\ \mu s \end{cases}$$

$u_k(t) \equiv 0$ for $k \neq 31$. (a) $1/g_2 = -20$ kΩ; stable. (b) $1/g_2 = -18$ kΩ; stable. (c) $1/g_2 = -17$ kΩ; unstable.

of the early vision chips, e.g., [7]–[14] and the networks considered in the present paper. Each node has conductance connections only with immediate neighbors. However, the MOS capacitors, nonlinearities of MOS conductances, and amplifiers in the input circuit could cause, depending on the design, oscillations. On the one hand, the problem in [6] is more difficult than the one discussed in this paper because nonlinearities must be taken into account. On the other hand, it is simpler in the sense that each node has connections only with its immediate neighbors. In [6] several sufficient conditions are given for temporal stability using a rather interesting argument. We close this section by noting that the observation was made in [15] that active conductances can cause instability in early vision neural networks.

II. Stability–Regularity

Subsection A explains how the temporal and the spatial dynamics are described. It is pointed out that the boundary

conditions should be carefully examined for the spatial dynamics. Subsection B characterizes the spatial dynamics in terms of the eigenspaces of the matrix describing the dynamics. The first main result, Theorem 1, clarifies conditions under which spatial responses behave properly. In particular, it states that in addition to a condition on the eigenvalues of the matrix describing the dynamics, another condition on the boundary is necessary. In subsection C the second main result, Theorem 2, reveals a fundamental relationship between the temporal and the spatial dynamics by showing that a network is temporally stable if and only if it is spatially regular, a new concept to be defined. Propositions 2 and 3 give the stability as well as the regularity criteria in terms of the characteristic polynomial of the matrix describing the spatial dynamics.

A. Formulation

Consider a neural network consisting of a linear array of n nodes where each node is connected with its pth nearest neighborhoods, $p = 1, \cdots, m < n$ via a (possibly negative) conductance g_p and a capacitance c_p. Fig. 5 shows the case where $m = 3$. The network is described by

$$\sum_{p \in M} b_p \frac{dv_{i-p}}{dt} = \sum_{p \in M} a_p v_{i-p} + u_i, \qquad i = 1, \cdots, n, \quad (1)$$

where v_i and u_i are the voltage and the input current at the ith node, and

$$M = \{p \text{ integer } ||p| \leq m\} \quad (2)$$

$$a_0 = -\left(g_0 + 2\sum_{p=1}^{m} g_p\right) \quad (3)$$

$$a_{\pm p} = g_p, \qquad 1 \leq p \leq m$$

$$b_0 = c_0 + 2\sum_{p=1}^{m} c_p \quad (4)$$

$$b_{\pm p} = -c_p, \qquad 1 \leq p \leq m.$$

Equation (1) is obtained simply by writing down the Kirchhoff's current law (KCL) at each node. Letting $\boldsymbol{v} = (v_1, \cdots, v_n)^T$ and $\boldsymbol{u} = (u_1, \cdots, u_n)^T$ (T denoting transpose), one can recast (1) as

$$\boldsymbol{B}\frac{d\boldsymbol{v}}{dt} = \boldsymbol{A}\boldsymbol{v} + \boldsymbol{u} \quad (5)$$

where

$$\boldsymbol{A} = \begin{bmatrix} a_0 & a_1 & \cdots & a_m & 0 & \cdots & 0 \\ a_1 & & & & & & 0 \\ \vdots & & & & & & a_m \\ a_m & & & & & & \vdots \\ 0 & & & & & & a_1 \\ \vdots & & & & & & a_0 \\ 0 & \cdots & 0 & a_m & \cdots & a_1 & \end{bmatrix} \quad (6)$$

$$\boldsymbol{B} = \begin{bmatrix} b_0 & b_1 & \cdots & b_m & 0 & \cdots & 0 \\ b_1 & & & & & & 0 \\ \vdots & & & & & & b_m \\ b_m & & & & & & \vdots \\ 0 & & & & & & b_1 \\ \vdots & & & & & & b_0 \\ 0 & \cdots & 0 & b_m & \cdots & b_1 & \end{bmatrix} \quad (7)$$

Note that $\boldsymbol{A}$ as well as $\boldsymbol{B}$ is symmetric and has a uniform band structure, which, as will be seen, yields interesting properties. If $\boldsymbol{B}$ is nonsingular, an equilibrium point of (5) satisfies

$$-\sum_{p \in M} a_p v_{i-p} = u_i \quad (8)$$

which is a difference equation instead of a differential equation. Assuming that $a_m \neq 0$, one has

$$v_{i+m} = -\frac{1}{a_m}\left(\sum_{p \in M - \{m\}} a_p v_{i+p} + u_i\right). \quad (9)$$

Therefore, letting

$$\boldsymbol{F} = \begin{bmatrix} 0 & 1 & 0 & \cdots & 0 \\ 0 & 0 & 1 & \cdots & 0 \\ \vdots & & \ddots & \ddots & \vdots \\ 0 & & & \ddots & 1 \\ -1 & -\frac{a_{m-1}}{a_m} & \cdots & -\frac{a_1}{a_m} & -\frac{a_0}{a_m} \end{bmatrix} \quad (10)$$

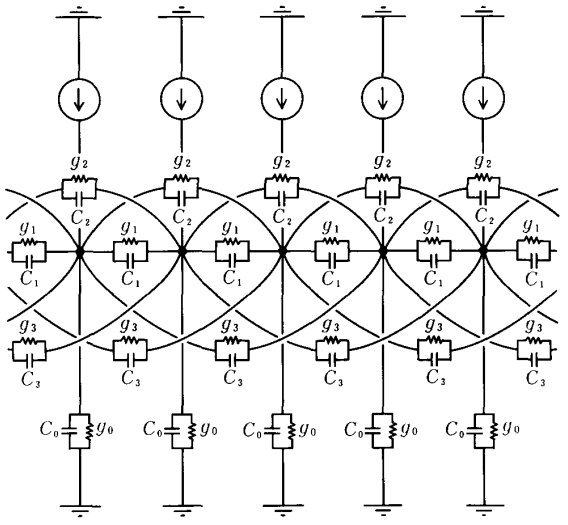

Fig. 5. Network described by (1) when $m = 3$.

with

$$\boldsymbol{x}_k = (v_{k-m}, v_{k-m+1}, \cdots, v_k, \cdots, v_{k+m-1})^T \in \mathbb{R}^{2m}$$
$$\boldsymbol{y}_k = (0, \cdots 0, -u_k/a_m)^T \in \mathbb{R}^{2m}$$

one can rewrite (9) as

$$\boldsymbol{x}_{k+1} = \boldsymbol{F}\boldsymbol{x}_k + \boldsymbol{y}_k \tag{11}$$

Observe that subscript k in (11) is not time. Equation (11) represents the *spatial dynamics* induced by the temporal dynamics (5). Note also that $\dim \boldsymbol{v} = n$, the number of nodes, while $\dim \boldsymbol{x}_k = 2m$, the size of the neighborhood, which is independent of n.

In image processing, input is $\boldsymbol{u}$ while output is $\boldsymbol{v}(\infty)$, the stable equilibrium point of (5). Equation (11) describes how the coordinates of $\boldsymbol{v}(\infty)$ are distributed with respect to k. There are several issues that need care.

First, the temporal dynamics given by (5) constitute an initial value problem while (8) or (11) is a boundary value problem. Namely, arbitrary $\boldsymbol{v}(0)$ and $\boldsymbol{u}(.)$ completely determine the solution to (5) while for (8) or (11), one *cannot* specify (for a given $\{\boldsymbol{y}_k\}$) an arbitrary $\boldsymbol{x}_0$ because a solution $\boldsymbol{x}_k$ must be consistent with the KCL's at the end points. Furthermore, the temporal dynamics given by (5) are *causal*; i.e., a solution at time t does not depend on the future. The spatial dynamics given by (11), however, are *noncausal*; i.e., a solution at node k depends on both the right-hand-side and left-hand-side neighbors. In order to be more specific, let us look at Fig. 6(a), where the right end point is shown with $m = 2$, $-K \le k \le K$, $n = 2K + 1$. Capacitors are omitted for the sake of simplicity. KCL's at the Kth and $(K-1)$th nodes are, respectively,

$$-(g_0 + g_1 + g_2)v_K + g_1 v_{K-1} + g_2 v_{K-2} = 0 \tag{12a}$$
$$-(g_0 + 2g_1 + g_2)v_{K-1} + g_1(v_K + v_{K-2}) + g_2 v_{K-3} = 0. \tag{12b}$$

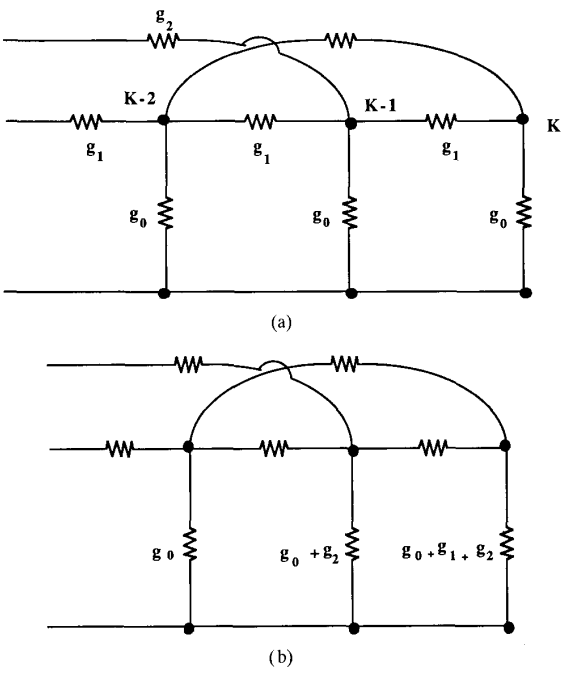

Fig. 6. Boundary conditions with $m = 2$ (a) The circuitry at the right end. (b) A modification of the boundary conditions establishes consistency.

The right-hand sides are nonzero when independent current sources are present. These equations define a two-dimensional linear subspace to which the boundary state $\boldsymbol{x}_K$ must belong. Another two-dimensional constraint is imposed at the left end. If these constraints are independent (generically they are), then a four-dimensional trajectory $\boldsymbol{x}_k \in \mathbb{R}^4$ is uniquely defined.

For a general m, there are m boundary conditions at the right end and there are another m conditions at the left end. An *impulse response* of (11), for instance, is determined in the following way. Let $\boldsymbol{y}_0 \neq \boldsymbol{0}$ whereas $\boldsymbol{y}_k = \boldsymbol{0}$ for $k \neq 0$ and consider $\boldsymbol{x}_0$, which is to be determined. Let $\mathbb{R}^{2m} \supset T_+$ (resp. T_-) be an m-dimensional linear subspace to which $\boldsymbol{x}_K$ (resp. $\boldsymbol{x}_{-K}$) must belong. Then

$$\boldsymbol{x}_K = F^K \boldsymbol{x}_0 + F^{K-1}\boldsymbol{y}_0 \in T_+ \tag{13a}$$

and

$$\boldsymbol{x}_{-K} = F^{-K}\boldsymbol{x}_0 \in T_-. \tag{13b}$$

determine $\boldsymbol{x}_0$ provided that T_+ and T_- are independent. Other $\boldsymbol{x}_k$'s are determined by

$$\boldsymbol{x}_k = \begin{cases} F^k \boldsymbol{x}_0 + F^{k-1}\boldsymbol{y}_0, & k \ge 1 \\ F^{-|k|}\boldsymbol{x}_0, & k \le -1 \end{cases}$$

Moving to the second issue, observe that the boundary conditions (12) are not consistent with the temporal dynamics (5) because the last two equations of an equilibrium are

$$-(g_0 + 2g_1 + 2g_2)v_n + g_1 v_{n-1} + g_2 v_{n-2} = 0 \tag{14a}$$
$$-(g_0 + 2g_1 + 2g_2)v_{n-1} + g_1(v_n + v_{n-2}) + g_2 v_{n-3} = 0. \tag{14b}$$

Here, we are slightly abusing our notations of K and n. There will be no confusion, however. The difference between (12) and (14) lies in the coefficients of the first terms. By a slight modification of circuit parameters, one can make (11) consistent with (5). That is, if one replaces the last two g_0's in Fig. 6(a) with $g_0 + g_1 + g_2$ and $g_0 + g_2$, respectively, as in Fig. 6(b), then it is consistent with (5). For a general m, one can maintain the consistency of (11) with (5) by replacing the last m g_0's by

$$g_0 + \sum_{p=1}^{m} g_p, \qquad g_0 + \sum_{p=2}^{m} g_p, \cdots, \qquad g_0 + g_m \tag{15}$$

respectively. We will assume, throughout, that this type of modification is always done.

The third issue is that the stability of the spatial dynamics (11) must be carefully defined. That "(11) is stable iff all the eigenvalues of $\boldsymbol{F}$ lie inside the unit circle" does not work because $\boldsymbol{F}$ has a special structure (see (42) below):

if λ is an eigenvalue, so is $1/\lambda$.

Therefore "$|\lambda| < 1$ for all λ" is never satisfied. Since $n = 2K + 1$ is *finite*, another standard definition of stability:

$$\sum_k \|\boldsymbol{y}_k\|^2 < \infty \text{ implies } \sum_k \|\boldsymbol{x}_k\|^2 < \infty \tag{16}$$

does not work either, because (16) is always satisfied. As was shown in Fig. 3(c), $\boldsymbol{x}_k$ can behave in a wild manner even if $n = 2K + 1$ is finite, which is highly undesirable for image processing purposes.

Finally, there is another problem concerning the finiteness of the network size n. Since $\boldsymbol{A}$ and $\boldsymbol{B}$ are symmetric, all eigenvalues are real. Thus, given a fixed n, while it is easy to *say* that (5) is asymptotically stable iff $\boldsymbol{B}^{-1}\boldsymbol{A}$ is negative definite, it is very hard to *derive* analytical (*a priori*) iff conditions for negative definiteness even with $m = 2$. One can derive, however, an interesting analytical condition if one looks for negative definiteness of $\boldsymbol{B}^{-1}\boldsymbol{A}$ *for all* n. Section III gives extremely simple analytical conditions for the temporal stability. With these conditions, a designer is guaranteed to have a stable network independent of the number of nodes. Without these conditions, a designer must compute all the eigenvalues of $\boldsymbol{B}^{-1}\boldsymbol{A}$. If one or more of the eigenvalues turn out to be nonnegative, one has to recompute the eigenvalues with a new trial set of parameter values. One also has to recompute eigenvalues when the network size is changed in response to certain design considerations.

Definition 1: A neural network described by (5) is said to be temporally stable if $\boldsymbol{B}^{-1}\boldsymbol{A}$ is negative definite for all n.

B. Spatial Dynamics

As was explained in subsection A, care needs to be exercised in studying the spatial dynamics (11). Let λ_{s_i}, λ_{c_i}, and λ_{u_i}, be the eigenvalues of $\boldsymbol{F}$ satisfying

$$|\lambda_{s_i}| < 1, \quad |\lambda_{c_i}| = 1 \quad \text{and} \quad |\lambda_{u_i}| > 1$$

respectively, and let E^s, E^c, and E^u be the (generalized) eigenspaces corresponding to λ_{s_i}, λ_{c_i}, and λ_{u_i}, respectively. They are called stable, center, and unstable eigenspaces, respectively. Let $E = \mathbb{R}^{2m}$. Then [16]

$$E = E^s \oplus E^c \oplus E^u \tag{17}$$

where $\oplus$ denotes a direct sum decomposition, and

$$\boldsymbol{F}(E^\alpha) = E^\alpha, \qquad \alpha = s, c, u, \tag{18}$$

i.e., E^s, E^c, and E^u are *invariant* under $\boldsymbol{F}$.

Our task here is to give an appropriate definition of spatial stability while maintaining consistency with (16) when $K \uparrow +\infty$.

Definition 2: A neural network described by (11) is said to be spatially stable if $\boldsymbol{F}$ is *hyperbolic,* i.e., if the center eigenspace E^c in (17) is empty.

Remark 1: Another way of saying this is that all the eigenvalues of $\boldsymbol{F}$ are off the unit circle. Of course, eigenvalues can be outside the unit circle. Note that this definition does not depend on the network size $n = 2K + 1$.

It is known that a noncausal linear system is stable in the sense of (16) iff its transfer function (in the frequency domain) has no poles on the unit circle. This, however, is when $K \uparrow +\infty$ and when there are no boundary conditions. One perhaps wants to argue (as, in fact, the authors did when they initiated the present study) that if the network size is sufficiently large, the behavior would be similar to that of the infinite case. This is simply wrong, as will be indicated by the following examples.

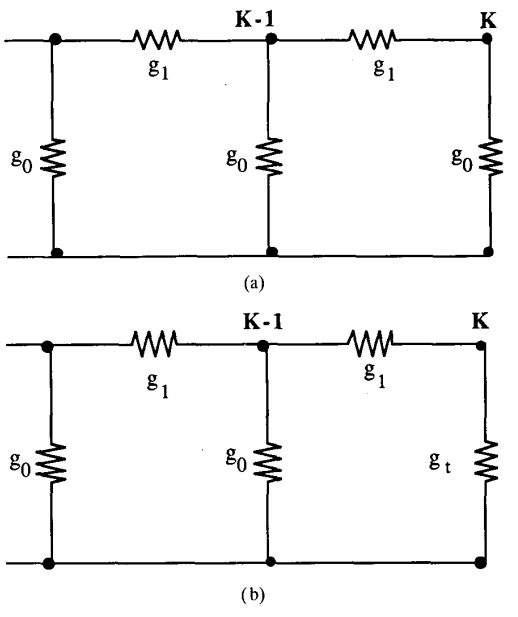

Fig. 7. A network with $m = 1$. (a) Original network. (b) Modified boundary condition, where the rightmost g_0 is replaced by g_t.

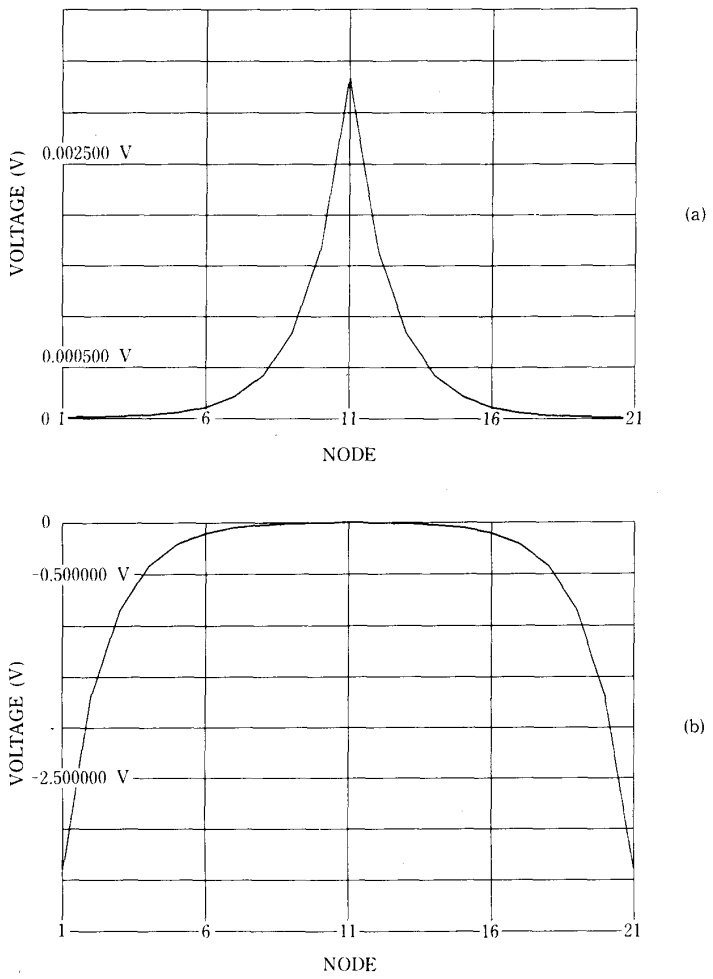

Fig. 8. Significance of boundary conditions. (a) Impulse response for Fig. 7(a) with $g_0 = g$, $g_1 = 2g$, $1/g = 50$ kΩ, $u_{31} = 0.1$ μA. (b) Impulse response for Fig. 7(b) with the same data except for $g_t = -g$, $u_{31} = 0.1$ μA.

Example 1: Consider the simplest case, $m = 1$ in (11) with $g_0 = g$, $g_1 = 2g$, $g > 0$ (Fig. 7(a)). Then

$$\boldsymbol{F} = \begin{bmatrix} 0 & 1 \\ -1 & \frac{5}{2} \end{bmatrix}$$

and $\boldsymbol{F}$ is hyperbolic because eigenvalues are $\lambda_1 = 1/2$ and $\lambda_2 = 2$. Fig. 8(a) shows the impulse response when $1/g = 50$ kΩ, where the impulse is injected at the center node. Let us now replace the rightmost g_0 and the leftmost g_0 with $g_t = -g$ as in Fig. 7(b). The impulse response is then given by Fig. 8(b), which "explodes" in the negative direction as $|k|$ increases. Note the difference of the voltage units. In both cases, the input current injected to the center node is the same and very small: 0.1 μA. It should be emphasized that the only difference is in the two g_t's, and the explosion happens in whichever way the network size is large. In fact, in our simulation with $n = 61$, an overflow occurred.

If the reader says that changing $g_t = g > 0$ to $-g < 0$ is unnatural, the following example shows the case in point.

Example 2: Consider Fig. 7(a) again with $g_0 = g > 0$ and $g_1 = -g/8$. Since eigenvalues of $\boldsymbol{F}$ are $-3 \pm 2\sqrt{2}$, $\boldsymbol{F}$ is hyperbolic, and Fig. 9(a) shows the impulse response with $1/g = 100$ kΩ. Next replace the rightmost and the leftmost g_0 with $g_t = g_0 - \left(g_0^2 + 4g_0g_1\right)^{1/2} = g\left(1 - 1/\sqrt{2}\right) > 0$ $(1/g_t \approx 341$ k$\Omega)$. The impulse response is given by Fig. 9(b), which again explodes. In both cases the input at the center node is 1 μA. Observe that since $g_1 < 0$ the stability issues are already nontrivial with $m = 1$. The stability issues for this example will be checked theoretically in Section III (see Example 5).

There is another story about spatial responses. Our simulation results indicate that spatial responses behave quite properly even if the g_t value is varied by a large amount. Namely, parts (a) and (b) of Fig. 3, Fig. 8(a), and Fig. 9(a) are very robust against variations of g_t from g_0.

Thus, two fundamental questions concerning the spatial dynamics must be answered:

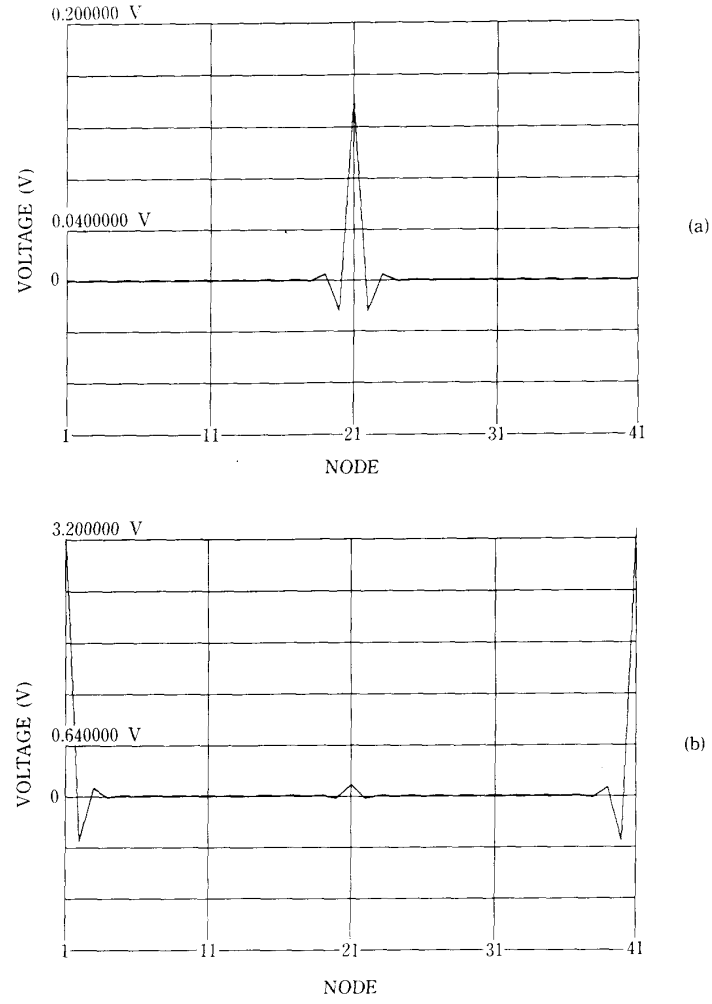

Fig. 9. Impulse response can explode even when $g_t > 0$. (a) Impulse response for Fig. 7(a) with $g_0 = g$, $g_1 = -g/8$, $1/g = 100$ kΩ, $u_{31} = 1$ μA. (b) Impulse response for Fig. 7(b) with the same data except for $g_t = g(1 - 1/\sqrt{2})$.

1) Why does a particular g_t value give rise to explosion of impulse responses even if the eigenvalues are off the unit circle?
2) Why do impulse responses behave properly over a wide range of g_t values?

One can answer the first question easily. Recall (13) and observe that a spatial response $\boldsymbol{x}_k$ depends not only on the input $\boldsymbol{y}_k$ but also on the boundary conditions T_+ and T_-. Therefore, if

$$T_+ = E^u \text{ (resp. } T_- = E^s) \tag{19}$$

then $\boldsymbol{x}_K$ (resp. $\boldsymbol{x}_{-K}$) is *forced* to lie in E^u (resp. E^s). Since E^u (resp. E^s) is invariant under $\boldsymbol{F}$, one has $\boldsymbol{x}_k \in E^u$ (resp. $\boldsymbol{x}_k \in E^s$) for *all* $k > 0$ (resp. $k < 0$); hence

$$\boldsymbol{x}_k = \lambda_2^k \boldsymbol{e}_2, \quad |\lambda_2| > 1, \quad \boldsymbol{e}_2 \in E^u, \quad k > 0$$
$$\left(\text{resp. } \boldsymbol{x}_k = \lambda_1^k \boldsymbol{e}_1, \quad |\lambda_1| < 1, \quad \boldsymbol{e}_1 \in E^s, \quad k < 0\right).$$

This means that $\boldsymbol{x}_k$ explodes as $|k|$ increases. For the network of Example 1 one can easily show that

$$E^u = \{(x_1, x_2) | 2x_1 - x_2 = 0\} \tag{20a}$$
$$E^s = \{(x_1, x_2) | x_1 - 2x_2 = 0\}. \tag{20b}$$

When $g_t = -g$ in Fig. 7(b), KCL at the Kth (resp. $-K$th) node reads $2gv_{K-1} - gv_K = 0$ (resp. $gv_{-K} - 2gv_{-K+1} = 0$), which implies (19). The situation is the same for Example 2. Another way of looking at Fig. 8(b) is to consider Fig. 10, where Fig. 10(a) is the original network and Fig. 10(b) shows that an equivalent conductance, $g_{\text{eq}}(K)$, as seen from node $K - 1$ is

$$g_{\text{eq}}(K) = (1/2g - 1/g)^{-1} = -2g.$$

Since $g + g_{\text{eq}}(K) = -g$, one sees that Fig. 10(b) is equivalent to Fig. 10(c); hence $g_{\text{eq}}(K - 1) = -2g$. It is clear that the equivalent conductance at any node k is $-2g$. This implies that KCL at every node $(k > 0)$ is $2gv_{k-1} - gv_k = 0$ so that

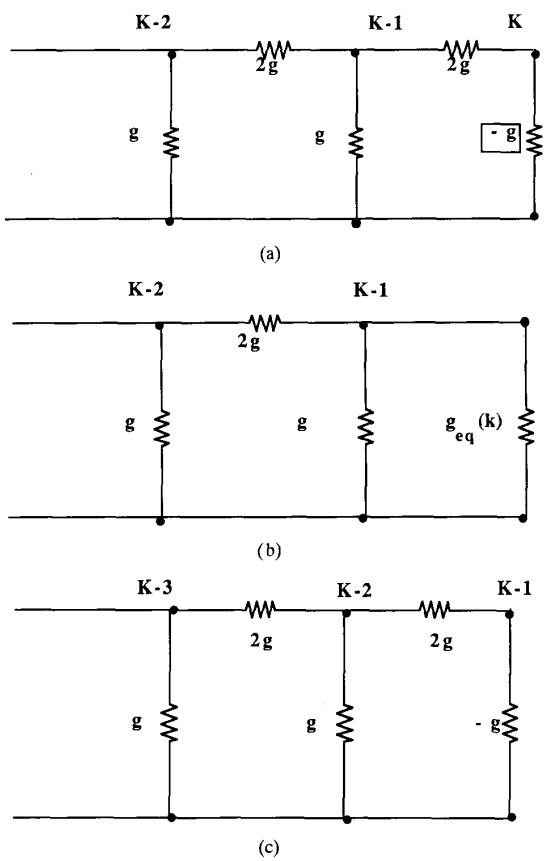

Fig. 10. An equivalent circuit of Fig. 7(b). (a) Original network. (b) The equivalent conductance $g_{\text{eq}}(K)$ seen from node $K-1$. (c) A circuit equivalent to Fig. 10(a).

$v_k = 2v_{k-1}$. Thus v_k explodes as $k > 0$ increases. A similar argument shows that v_k, $k < 0$, also explodes as k decreases. The situation in Example 2 is the same.

Answering the second question is much harder. The arguments used in answering the first question cannot be used here. Instead, it exemplifies the difficulty. Observe that KCL at the Kth node in Fig. 7(a) for Example 1 is

$$T_+ : -3gv_K + 2gv_{K-1} = 0$$

and hence

$$T_+ \neq E^u, \qquad T_+ \neq E^s \tag{21a}$$
$$T_- \neq E^u, \qquad T_- \neq E^s. \tag{21b}$$

These facts imply that the response $\boldsymbol{x}_k$ is of the form

$$\boldsymbol{x}_k = \lambda_1^k \boldsymbol{e}_1^+ + \lambda_2^k \boldsymbol{e}_2^+, \qquad k > 0 \tag{22a}$$
$$\boldsymbol{x}_k = \lambda_1^k \boldsymbol{e}_1^- + \lambda_2^k \boldsymbol{e}_2^-, \qquad k < 0 \tag{22b}$$

where $\boldsymbol{e}_1{}^{\pm}$ (resp. $\boldsymbol{e}_2^{\pm}$) are the eigenvectors associated with λ_1 (resp. λ_2) and all of them are *nonzero*. The situation given by (21) does not change for a wide range of g_t variations. This means that there is always an *expanding* term $\lambda_2^k \boldsymbol{e}_2^+$ (resp. $\lambda_1^k \boldsymbol{e}_1^-$) in (22a) (resp. (22b)), in addition to the decaying term $\lambda_1^k \boldsymbol{e}_1^+$ (resp. $\lambda_2^k \boldsymbol{e}_2^-$). This raises another serious question. Consider Example 1 again with $g_t = g > 0$. Since everything is passive, our intuition demands that there should be no stability problems. Nevertheless, (22) says that there are expanding terms.

Thus, another question arises: How can (22) involve expanding terms when everything is passive? In order to answer this, let us first consider the case where the network size is infinite and no boundary conditions are imposed. Let $\{\bar{\boldsymbol{x}}_k\}_{-\infty}^{+\infty}$ be the impulse response defined by

$$\bar{\boldsymbol{x}}_{k+1} = \boldsymbol{F}\bar{\boldsymbol{x}}_k, \qquad k \neq 0$$
$$\bar{\boldsymbol{x}}_1 = \boldsymbol{F}\bar{\boldsymbol{x}}_0 + \boldsymbol{y}_0.$$

Then the network is stable in the sense of (16) only if for every $\boldsymbol{y}_0$

$$\left\|\boldsymbol{F}^k \bar{\boldsymbol{x}}_1\right\| \to 0 \qquad \text{as } k \uparrow +\infty$$
$$\left\|\boldsymbol{F}^k \bar{\boldsymbol{x}}_0\right\| \to 0 \qquad \text{as } k \downarrow -\infty.$$

It will be shown later that this is possible only if E^c, the center eigenspace of $\boldsymbol{F}$, is empty. In order to see distinctions between solutions with and without boundary conditions more precisely, note that in image processing, the input $\{\boldsymbol{y}_k\}$ in (11) is not an impulse, but nonzero for $0 \leq k \leq d$.

Definition 3: Consider (11) and let $\{\boldsymbol{y}_k\}$ be nonzero only for $0 \leq k \leq d$. Then $\{\bar{\boldsymbol{x}}_k\}_{-\infty}^{+\infty}$ is said to be a *free-boundary solution* if

$$\bar{\boldsymbol{x}}_{k+1} = \boldsymbol{F}\bar{\boldsymbol{x}}_k, \qquad k < 0 \tag{23a}$$
$$\bar{\boldsymbol{x}}_d = \boldsymbol{F}^d \bar{\boldsymbol{x}}_0 + \sum_{k=0}^{d-1} \boldsymbol{F}^{d-k}\boldsymbol{y}_k \tag{23b}$$
$$\bar{\boldsymbol{x}}_{k+1} = \boldsymbol{F}\bar{\boldsymbol{x}}_k, \qquad k \geq d. \tag{23c}$$

Remark 2: If $d = 1$, then $\{\boldsymbol{y}_k\}$ is an impulse. If one redefines the summation term in (23b) as a new $\boldsymbol{y}_0$, then (23) can be replaced by

$$\bar{\boldsymbol{x}}_{k+1} = \boldsymbol{F}\bar{\boldsymbol{x}}_k, \qquad k \neq 0 \tag{24a}$$
$$\bar{\boldsymbol{x}}_1 = \boldsymbol{F}^d \bar{\boldsymbol{x}}_0 + \boldsymbol{y}_0. \tag{24b}$$

Since no boundary conditions are imposed, $\{\bar{\boldsymbol{x}}_k\}_{-\infty}^{+\infty}$ is not unique. The following proposition clarifies the uniqueness issue in terms of stability. Let

$$\lambda_{\max} := \max\{|\lambda_{\text{si}}| \mid \lambda_{\text{si}} \text{ is a stable eigenvalue}\}$$
$$\lambda_{\min} := \min\{|\lambda_{\text{ui}}| \mid \lambda_{\text{ui}} \text{ is an unstable eigenvalue}\}$$
$$\lambda_{\#} := \min\left(\lambda_{\min}, \lambda_{\max}^{-1}\right). \tag{25}$$

Proposition 1:

i) The $\boldsymbol{F}$ matrix of the spatial dynamics is hyperbolic if and only if for any $\boldsymbol{y}_0$ there is a unique free-boundary solution $\{\bar{\boldsymbol{x}}_k\}_{-\infty}^{+\infty}$ satisfying

$$\sum_{k=-\infty}^{+\infty} \|\bar{\boldsymbol{x}}_k\|^2 < \infty. \tag{26}$$

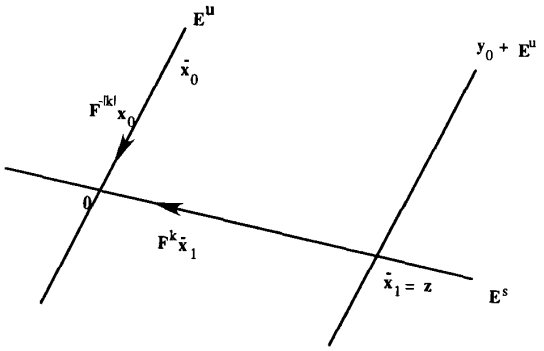

Fig. 11. Definition of z.

ii) The unique $\{\bar{\boldsymbol{x}}_k\}_{-\infty}^{+\infty}$ is determined by

$$\bar{\boldsymbol{x}}_1 \in E^s, \qquad \bar{\boldsymbol{x}}_0 \in E^u, \qquad \bar{\boldsymbol{x}}_1 = F^d \bar{\boldsymbol{x}}_0 + \boldsymbol{y}_0. \tag{27}$$

Proof:

i) $\Rightarrow$) Since E^c is empty (see (17)),

$$E = E^u \oplus E^s.$$

Since E^u is invariant under $\boldsymbol{F}$ (see (18)),

$$\left(\boldsymbol{F}^d E^u + \boldsymbol{y}_0\right) \cap E^s = (E^u + \boldsymbol{y}_0) \cap E^s \tag{28}$$

and this intersection is a singleton set, say $\{\boldsymbol{z}\}$ (Fig. 11). Define

$$\bar{\boldsymbol{x}}_0 := \boldsymbol{F}^{-d}(\boldsymbol{z} - \boldsymbol{y}_0), \qquad \bar{\boldsymbol{x}}_1 := \boldsymbol{z} \tag{29}$$

and let other $\bar{\boldsymbol{x}}_k$ be defined by (24a). Then

$$\begin{aligned} \sum_{k=-\infty}^{+\infty} \|\bar{\boldsymbol{x}}_k\|^2 &= \sum_{k=-\infty}^{0} \|\bar{\boldsymbol{x}}_k\|^2 + \sum_{k=1}^{\infty} \|\bar{\boldsymbol{x}}_k\|^2 \\ &\le \sum_{k=0}^{\infty} \lambda_{\#}^{-2k} \|\bar{\boldsymbol{x}}_0\|^2 + \sum_{k=1}^{\infty} \lambda_{\#}^{-2k} \|\bar{\boldsymbol{x}}_1\|^2 \\ &= \frac{\lambda_{\#}^2}{\lambda_{\#}^2 - 1} \|\bar{\boldsymbol{x}}_0\|^2 + \frac{1}{\lambda_{\#}^2 - 1} \|\bar{\boldsymbol{x}}_1\|^2 < \infty \end{aligned} \tag{30}$$

where $\lambda_{\#}$ is defined by (25). Note that (29) is equivalent to (27) and this is the only choice of $\bar{\boldsymbol{x}}_1$ and $\bar{\boldsymbol{x}}_0$ for which (26) holds, because if $\bar{\boldsymbol{x}}_1 \notin E^s$, for instance, then $\bar{\boldsymbol{x}}_1 = \bar{\boldsymbol{x}}_1^u + \bar{\boldsymbol{x}}_1^s$, with nonzero $\bar{\boldsymbol{x}}_1^u$. Hence $\left\|\boldsymbol{F}^k \bar{\boldsymbol{x}}_1^u\right\| \to \infty$ as $K \uparrow +\infty$. A similar argument holds for $\bar{\boldsymbol{x}}_0$.

$\Leftarrow$) If E^c is non-empty, then there is a $\boldsymbol{y}_0 \neq \boldsymbol{0}$ such that $(E^u + \boldsymbol{y}_0) \cap E^s = \phi$. It is clear that for such $\boldsymbol{y}_0$ there is no way of choosing $\bar{\boldsymbol{x}}_1$ and $\bar{\boldsymbol{x}}_0$ which satisfy (26).

ii) Clearly, (27) and (29) are equivalent. □

Definition 4: The unique $\{\bar{\boldsymbol{x}}_k\}_{-\infty}^{+\infty}$ given in Proposition 1 is said to be the *stable* free-boundary solution.

Remark 3:

i) Consider a free-boundary solution for Example 1, i.e., when $g_0 = g$ and $g_1 = 2g$ extending indefinitely. In spite of the fact that everything is passive, exploding solutions are mathematically legitimate. However, by demanding the finite total energy (26), one forces all exploding solutions to be illegitimate and makes only one solution legitimate, which is given by (27). Conversely, if a unique stable free-boundary solution exists, then the $\boldsymbol{F}$ matrix must satisfy hyperbolicity.

ii) The stable free-boundary solution in terms of (21) can be characterized as $\boldsymbol{e}_2^+ = \boldsymbol{e}_1^- = \boldsymbol{0}$.

Recall the boundary conditions T_+ and T_- in (13).

Definition 5: Let $\{\boldsymbol{y}_k\}$ be nonzero only for $0 \le k \le d$. Then $\{\boldsymbol{x}_k\}_{-K}^{+K}$ is said to be a *solution for* (T_+, T_-, K) if

$$\boldsymbol{x}_{k+1} = \boldsymbol{F}\boldsymbol{x}_k, \qquad -K \le k \le K, \qquad k \neq 0, \tag{31}$$

$$\boldsymbol{x}_1 = \boldsymbol{F}^d \boldsymbol{x}_0 + \boldsymbol{y}_0 \tag{32}$$

$$\boldsymbol{x}_{-K} \in T_-, \qquad \boldsymbol{x}_K \in T_+. \tag{33}$$

The following result thoroughly answers the second and third questions that arose in connection with spatial dynamics in a very general setting.

Theorem 1: Let a neural network described by (11) be spatially stable, i.e., let $\boldsymbol{F}$ be hyperbolic. If the boundary conditions T_+ and T_- satisfy

$$T_+ + E^u = E, \qquad T_- + E^s = E \tag{34}$$

then a solution $\{\boldsymbol{x}_k\}_{-K}^{+K}$ for (T_+, T_-, K) converges to the stable free-boundary solution $\{\bar{\boldsymbol{x}}_k\}_{-\infty}^{+\infty}$ as $K \uparrow +\infty$:

$$\lim_{K \to +\infty} \sum_{k=-K}^{+K} \|\bar{\boldsymbol{x}}_k - \boldsymbol{x}_k\|^2 = 0. \tag{35}$$

Proof: See Appendix I.

Remark 4:

i) In words, this theorem tells us that if the $\boldsymbol{F}$ matrix of the spatial dynamics satisfies the spatial stability condition (Definition 2) and, in addition, if the boundary conditions satisfy (34), then response $\boldsymbol{x}_k$ not only behaves properly but also converges to the stable free-boundary solution $\bar{\boldsymbol{x}}_k$ as $K \uparrow +\infty$.

ii) It will be shown in subsection III-B (see Example 3) that for parts (a) and (b) of Fig. 3, $\boldsymbol{F}$ is hyperbolic while for Fig. 3(c), it is nonhyperbolic. A simple computation shows that there are two distinct pairs of complex conjugate eigenvalues on the unit circle for Fig. 3(c).

iii) Since T_+, T_-, E^u, and E^s all have the same dimension m, the vector sum $+$ in (34) amounts to the same

as the direct sum $\oplus$. Therefore, dim T_+ + dim E^u = dim E and dim T_- + dim E^s = dim E; hence condition (34) is extremely mild. It is satisfied *unless* $\boldsymbol{x}_K$ (resp. $\boldsymbol{x}_{-K}$) is forced to lie in E^u (resp. E^s). This explains why all of our computer simulations look the same with various boundary conditions except for peculiar ones. What happens if T_+ (resp. T_-) is very close to E^u (resp. E^s)? This simply requires a very large K to observe a solution similar to the stable free-boundary solution.

iv) Since E^c is empty, $\boldsymbol{x}_1$defined by (32) can be written as

$$\boldsymbol{x}_1 = \boldsymbol{x}_1^u + \boldsymbol{x}_1^s, \qquad \boldsymbol{x}_1^u \in E^u, \qquad \boldsymbol{x}_1^s \in E^s. \tag{36}$$

A crucial step in the proof of Theorem 1 given in Appendix I is to obtain estimates on $\left\|\boldsymbol{F}^k\boldsymbol{x}_1^u\right\|$, $k \geq 0$, and $\left\|\boldsymbol{F}^k\boldsymbol{x}_0^s\right\|$, $k \leq 0$, because these terms are expanding instead of decaying. The following is roughly what is happening. Let $\{\boldsymbol{x}_k\}_{-K}^{+K}$ be a solution for (T_+, T_-, K), and let $K < K'$ while T_+ and T_- are fixed. In order for $\{\boldsymbol{x}_k\}_{-K'}^{+K'}$ to be a solution for (T_+, T_-, K'), it must make more iterations to reach T_+ from $\boldsymbol{x}_1'$ than that for $\{\boldsymbol{x}_k\}_{-K}^{+K}$. There are two ways to do this. In the first, $\boldsymbol{x}_1'$ locates itself farther away from the origin than $\boldsymbol{x}_1$. In a second, $\boldsymbol{x}_{K'}$ hits T_+ at a point closer to the origin than $\boldsymbol{x}_K$ does (Fig. 12). There is a limitation to the first method because $\boldsymbol{x}_1'$ must satisfy (32) while $\boldsymbol{y}_0$ and d are *fixed.* On the other hand, there is no such limitation to the second method because the dynamics can get as "slow" as it pleases as the origin is approached.[1] This allows one to give an appropriate estimate on $\left\|\boldsymbol{F}^k\boldsymbol{x}_1\right\|$, $k \geq 0$. A similar argument holds for T_-.

v) It is rather interesting to observe that the network given in Example 1 is exactly a D/A converter widely used in practice. See [17] for instance. The network is called the R–$2R$ ladder because $g_0 = g$ and $g_1 = 2g$. In order to convert an n-bit binary signal into an analog signal, one inputs a constant current source at the kth node if the kth bit is "1"; otherwise the current source is set to zero. In such a D/A converter, the rightmost g_0 is replaced with $g_t = 2g$ instead of[2] g so that KCL gives $v_{K-1} - 2v_K = 0$, which forces (see (20b))

$$\boldsymbol{x}_K \in E^s. \tag{37}$$

Since E^s is invariant and since the stable eigenvalue is $1/2$, one has $\boldsymbol{x}_K = \left(1/2^{(K-k)}\right)\boldsymbol{x}_k$. If the leftmost g_t is $2g$ also, then $\boldsymbol{x}_{-K} \in E^u$. Any response of a linear network is a superposition of impulse responses, hence the rightmost voltage v_K, which is the output, is given as

$$v_K = \text{constant} \times \sum_k 1/2^k \tag{38}$$

where k runs over those nodes where "1" is present. Note that if g_t were not chosen as $2g$, the D/A converter would give a wrong analog output.

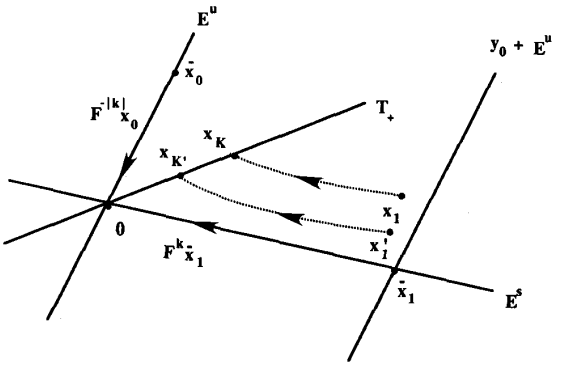

Fig. 12. An illustration of the proof of Theorem 1.

C. Temporal Stability—Spatial Regularity

Now we turn to the relationship between the temporal and the spatial dynamics for which a new concept is needed.

Definition 6: A neural network described by (11) is said to be *spatially regular* if there is a nonsingular $2m \times 2m$ matrix $\boldsymbol{T}$ such that

$$\boldsymbol{TFT}^{-1} = \begin{array}{c} \boldsymbol{E}^s \oplus \boldsymbol{E}^c \oplus \boldsymbol{E}^u \\ \left[\begin{array}{c|c|c} \boldsymbol{F}_s & & \\ \hline & \boldsymbol{F}_c \quad \boldsymbol{G} & \\ \hline & \boldsymbol{F}_c & \boldsymbol{F}_s^{-1} \end{array}\right] \end{array} \tag{39}$$

where a blank indicates a zero matrix, and elements of $\boldsymbol{G}$ consist of $+1$ or 0.

Remark 5: Spatial regularity demands several particular structures in the dynamics:

i) dim E^s = dim E^u and

$$\boldsymbol{F}|E^u = (\boldsymbol{F}|E^s)^{-1} \tag{40}$$

where $\boldsymbol{F}|E^u$ (resp. $\boldsymbol{F}|E^s$) denotes the restriction of $\boldsymbol{F}$ to E^u (resp. E^s). Namely, the dynamics on the unstable eigenspace E^u are exactly the same as the inverse dynamics on the stable eigenspace E^s.

ii) The center eigenspace E^c is decomposed as $E^{c1} \oplus E^{c2}$, dim E^{c1} = dim E^{c2}, and $\boldsymbol{F}|E^{c1}$ and $\boldsymbol{F}|E^{c2}$ have essentially the same structure.

iii) If a neural network described by (11) is spatially stable, E^c is empty. It will be shown later (see (43)) that (40) is satisfied for (10). Therefore, spatial stability *implies* spatial regularity, *but not conversely.*

The following standing assumptions are made throughout the paper unless stated otherwise.

Standing Assumptions: In (5),

(i) $a_0 < 0$, $a_m \neq 0$;

[1] The dynamics $\boldsymbol{x}_{k+1} = \boldsymbol{F}\boldsymbol{x}_k$ have "zero" speed at the origin because $\boldsymbol{F0} = \boldsymbol{0}$; i.e., it does not move. Since a solution depends continuously on its initial condition, one sees that the dynamics gets slower without limit as it approaches the origin.

[2] Recall that in Fig. 8(a) $g_t = g$, while in Fig. 8(b) $g_t = -g$.

(ii) $\boldsymbol{B}$ is positive definite for all n.

Since we are looking for conditions under which $\boldsymbol{B}^{-1}\boldsymbol{A}$ is negative definite for all n, the diagonal element a_0 of $\boldsymbol{A}$ must be negative (provided that $\boldsymbol{B}$ is positive definite), which is the inequality in (i). If $a_m = 0$, then the neighborhood M is of a smaller size. No restrictions will be imposed on the sign of a_p, $p \neq 0$. In image processing neuro chips, c_p in (4) are parasitic capacitors of MOS processes, and positive definiteness of $\boldsymbol{B}$ is a mild condition. The following result establishes a fundamental relationship between the temporal and spatial dynamics.

Theorem 2: A neural network described above is temporally stable *if and only if* it is spatially regular.

Proof: Consider the characteristic polynomial of $\boldsymbol{F}$:

$$P_F(\lambda) := \det(\lambda \mathbf{1} - \boldsymbol{F}) = \lambda^m \left[\frac{a_0}{a_m} + \sum_{p=1}^{m} \frac{a_p}{a_m} \left(\lambda^p + \lambda^{-p} \right) \right] \tag{41}$$

which satisfies

$$P_F(\lambda) = \lambda^{2m} P_F\left(\frac{1}{\lambda} \right). \tag{42}$$

This implies that if λ_s (resp. λ_u) is a stable (resp. unstable) eigenvalue, i.e., $|\lambda_s| < 1$ (resp. $|\lambda_u| > 1$), then λ_s^{-1} (resp. λ_u^{-1}) is also an eigenvalue and unstable (resp. stable). $\boldsymbol{F}$ is nonsingular, for $\det \boldsymbol{F} = 1$; hence there are no zero eigenvalues. This implies that $\dim E^s = \dim E^u$ and

$$\boldsymbol{F}|E^u = (\boldsymbol{F}|E^s)^{-1}. \tag{43}$$

In order to discuss $\boldsymbol{F}|E^c$, let

$$\omega = \lambda + \lambda^{-1} \quad \text{or} \quad \lambda = \frac{1}{2}\left(\omega \pm \sqrt{\omega^2 - 4} \right). \tag{44}$$

By a repeated use of the binomial formula:

$$\lambda^{2p} + \lambda^{-2p} = \omega^{2p} - \sum_{i=1}^{p-1} {}_{2p}C_i \left[\lambda^{2(p-i)} + \lambda^{-2(p-i)} \right] - {}_{2p}C_p$$

$$\lambda^{2p+1} + \lambda^{-(2p+1)} = \omega^{2p+1} - \sum_{i=1}^{p} {}_{2p+1}C_i \left[\lambda^{2(p-i)+1} + \lambda^{-2(p-i)-1} \right]$$

one sees that

$$\frac{a_0}{a_m} + \sum_{p=1}^{m} \frac{a_p}{a_m} \left(\lambda^p + \lambda^{-p} \right) = \sum_{p=0}^{m} \alpha_p \omega^p := Q(\omega) \tag{45}$$

for real α_p's. Since $\boldsymbol{F}$ has no zero eigenvalues,

$$P_F(\lambda) = 0 \quad \text{iff } Q(\omega) = 0 \tag{46}$$

where λ and ω are related via (44). Hence if λ_c is *real* and $|\lambda_c| = 1$, then (44) forces λ_c to be a *double* eigenvalue $\{\lambda_c, \lambda_c\}$ or its *multiple*. We next claim that

$$\dim \ker(\lambda \mathbf{1} - \boldsymbol{F}) = 1 \tag{47}$$

for any eigenvalue λ, where "ker" denotes the kernel of a matrix. In order to see this, note first that λ being an eigenvalue implies

$$\det(\lambda \mathbf{1} - \boldsymbol{F}) = 0.$$

The determinant of the $(2m-1) \times (2m-1)$ principal minor of $\lambda \mathbf{1} - \boldsymbol{F}$ is given by

$$\det \begin{bmatrix} \lambda & 1 & & & \\ & \lambda & 1 & & \\ & & \ddots & \ddots & \\ & & & \lambda & 1 \\ & & & & \lambda \end{bmatrix} = \lambda^{(2m-1)} \neq 0$$

because $\boldsymbol{F}$ has no zero eigenvalues. This shows (47). Thus, for each eigenvalue λ of $\boldsymbol{F}$, there is *only one elementary Jordan block* [16]. Therefore the *real canonical form* of $\boldsymbol{F}|E^{\lambda_c}$ restriction of $\boldsymbol{F}$ to the eigenspace corresponding to λ_c, is given by

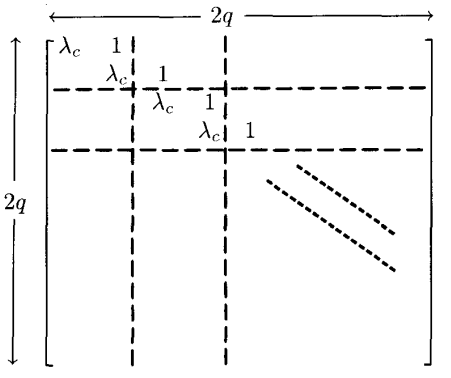

(48)

where $2q$ is the multiplicity. This is clearly of the form (39).

So far, no use has been made of the negative definiteness of $\boldsymbol{B}^{-1}\boldsymbol{A}$ and yet we are already close to (39), the regularity. The situation, however, is slightly subtle when it comes to a *nonreal* λ_c with $|\lambda_c| = 1$, because (42) tells us nothing except for the fact that λ_c^*, the complex conjugate, is also an eigenvalue. This last is of no use since $\boldsymbol{F}$ is a real matrix and λ_c^* also being an eigenvalue is automatic. We now assume that $\boldsymbol{B}^{-1}\boldsymbol{A}$ is negative definite for all n. Since $\boldsymbol{B}$ is positive definite for all n, $\boldsymbol{A}$ is negative definite for all n. It is known [18], then, that there are $z_p \in \mathbb{R}$, $p = 0, \cdots, m$, such that the elements of $\boldsymbol{A}$ satisfy

$$-a_p = \sum_{i=0}^{m-p} z_i z_{i+p}, \qquad p = 0, \cdots, m \tag{49}$$

i.e., a_p's can be decomposed as in (49). Substitution of (49) into (41) yields

$$P_F(\lambda) = -\frac{\lambda^m}{z_0 z_m} \left[\sum_{i=0}^{m} z_i^2 + \sum_{p=1}^{m} \sum_{i=0}^{m-p} z_i z_{i+p} \left(\lambda^i + \lambda^{-i} \right) \right]$$

$$= -\frac{\lambda^m}{z_0 z_m} \left(\sum_{i=0}^{m} z_i \lambda^{-i} \right) \left(\sum_{i=0}^{m} z_i \lambda^{-i} \right). \tag{50}$$

Since $0 \neq a_m = -z_0 z_m$ and since $\boldsymbol{F}$ has no zero eigenvalues, one sees that

$$P_F(\lambda) = 0 \quad \text{iff } R(\lambda) R\left(\frac{1}{\lambda} \right) = 0 \tag{51}$$

where

$$R(\lambda) = \sum_{i=0}^{m} z_i \lambda^i. \tag{52}$$

Therefore if λ is a nonreal eigenvalue with $|\lambda_c| = 1$, (51) forces the eigenvalue configuration to be of the form $\{\lambda_c, \lambda_c^*, \lambda_c, \lambda_c^*\}$ or its *multiple*. It follows from (47) that the real canonical form of $\boldsymbol{F}$ on this eigenspace is given by

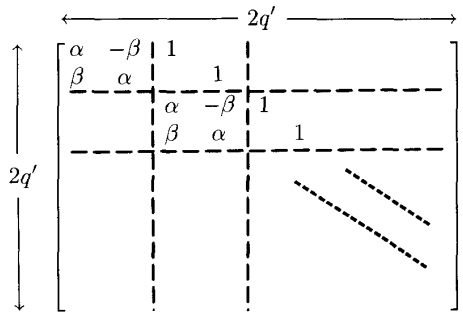

(53)

where

$$\alpha^2 + \beta^2 = 1 \tag{54}$$

and $2q'$ is the multiplicity. This, again, is of the form (39).

If a neural network is spatially regular, the real canonical form of the spatial dynamics $\boldsymbol{F}$ is equivalent to (39). The characteristic polynomial of $\boldsymbol{F}$, then, admits a decomposition of the form given by (50). Comparing (50) with (45), one sees that (49) holds. This condition is known [18] to be not only a necessary but also a sufficient condition for $\boldsymbol{A}$ to be negative definite for all n. Since $\boldsymbol{B}$ is positive definite and symmetric for all n, it follows from [19] that

$$\text{max. eigenvalue of } \boldsymbol{B}^{-1}\boldsymbol{A} = \max_{\boldsymbol{v}\neq 0} \frac{\boldsymbol{v}^T\boldsymbol{A}\boldsymbol{v}}{\boldsymbol{v}^T\boldsymbol{B}\boldsymbol{v}} < 0 \tag{55}$$

for any n which implies temporal stability. □

Remark 6: Suppose that a neural network is temporally stable. Although its spatial dynamics can be unstable, it has a sort of symmetry in that the spatial dynamics cannot have a component which is essentially different from the rest; i.e., every component has its partner.

Remark 7:

i) Consider (1) and let

$$W := \sum_{i=1}^{n} v_i u_i$$

which is the *power* injected into the network. It follows from (1) that

$$\begin{aligned} W &= -\sum_i \sum_p v_i a_p v_{i-p} + \sum_i \sum_p v_i b_p \frac{dv_{i-p}}{dt} \\ &= -\boldsymbol{v}^T\boldsymbol{A}\boldsymbol{v} + \boldsymbol{v}^T\boldsymbol{B}\frac{d\boldsymbol{v}}{dt} \\ &:= W_R + W_C. \end{aligned}$$

Thus the first term

$W_R = -\boldsymbol{v}^T\boldsymbol{A}\boldsymbol{v}$ = power dissipated by the resistive part of the network. Therefore a neural network is temporally stable iff its resistive part is *strictly passive,* i.e.,

$$W_R > 0, \qquad \boldsymbol{v} \neq 0 \qquad \text{for all } n.$$

ii) It follows from the previous remark that spatial stability demands more than strict passivity of the resistive part.

iii) Observe that

$\boldsymbol{v}^T\boldsymbol{B}\boldsymbol{v}/2$ = energy stored in the capacitors.

Therefore (55) says that

$$\begin{aligned} &\text{max. eigenvalue of } \boldsymbol{B}^{-1}\boldsymbol{A} \\ &= \max\left(\frac{-\text{power dissipated by resistors}}{2 \cdot \text{ energy stored in capacitors}}\right) \\ &= -\min\left(\frac{\text{power dissipated by resistors}}{2 \cdot \text{ energy stored in capacitators}}\right). \end{aligned}$$

Remark 8: Since the capacitance matrix $\boldsymbol{B}$ has exactly the same structure as that of $\boldsymbol{A}$, one can derive an iff condition for its positive definiteness. If all c_p's are positive, however, then the positive definiteness is straightforward because

$$b_0 = c_0 + 2\sum_{p=1}^{m} c_p > 2\sum_{p=1}^{m} c_p = 2\sum_{p=1}^{m} |b_p| \tag{56}$$

i.e., the diagonal element is larger than the sum of the row elements. Since $\boldsymbol{B}$ is symmetric, this implies positive definiteness.

Remark 9: Since an actual chip is made up of MOS transistors, the formulation given by (1)–(4) is naturally a model. For example, in [1] both the variable conductance g_0 and the negative conductance g_2 are composite CMOS circuits. As one of the reviewers correctly points out, a reasonable justification of the model should be given. Appendix VII supplies a justification.

Now the question naturally arises as to how one checks temporal stability or spatial regularity. Since temporal stability is equivalent to spatial regularity, we will say, hereafter, that the *stability–regularity* condition is satisfied if a network is temporally stable or spatially regular. Recall $Q(\omega)$ defined by (45).

Proposition 2: The following are equivalent:

i) Stability–regularity.

ii) Every nonreal eigenvalue λ_c of $\boldsymbol{F}$ with $|\lambda_c| = 1$ has an even multiplicity.

iii) Every real zero ω_R of Q with $|\omega_R| < 2$ has an even multiplicity.

Proof: Equivalence between (i) and (ii) was demonstrated in the proof of Theorem 2. To show that (ii) and (iii), suppose that $\lambda_c = e^{j\theta}$, $\theta \neq k\pi$, is an eigenvalue of $\boldsymbol{F}$. Then (44) implies that the corresponding ω is real and $|\omega| < 2$. Conversely, if ω is real and $|\omega| < 2$, then (44) says that $\lambda_c = e^{\pm j\theta}$, $\theta \neq k\pi$. □

For the sake of the completeness, we will state the following:

Proposition 3: The following are equivalent:

i) Spatial stability.

ii) Eigenvalues of $\boldsymbol{F}$ are off the unit circle.
iii) Q has no real zero on $[-2, 2]$.

III. Explicit Stability Criteria

Even though both conditions (ii) and (iii) of Proposition 2 give a specific way of checking the stability–regularity, explicit analytical conditions in terms of the circuit parameters greatly help in designing circuits. The same is true for the spatial stability. In subsection III-A two stability indicator functions will be given for a general m, with which one can easily check the stability–regularity or the spatial stability in terms of circuit parameters. In subsections B through D, the stability indicator functions will be specialized to $m \leq 3$. In particular, it will be shown that the conductance values of the neuro chip which motivated the present study satisfy the temporal as well as the spatial stability conditions. Furthermore, it will be rigorously shown why our numerical experiments indicated the "equivalence" between the temporal and the spatial stability.

A. Stability Indicator Functions

The following functions play a crucial role throughout the rest of the paper and will be called the stability indicator functions:

$$\begin{aligned} \sigma_+(a_0, a_1, \cdots, a_m) &:= \max_{\omega \in [-2,2]} a_m Q(\omega) \\ \sigma_-(a_0, a_1, \cdots, a_m) &:= \min_{\omega \in [-2,2]} a_m Q(\omega) \end{aligned} \tag{57}$$

where Q is defined by (45).

Proposition 4: A neural network described by (5) and (11) satisfies the stability–regularity condition *if and only if*

$$\sigma_+(a_0, a_1, \cdots, a_m) \leq 0. \tag{58}$$

Proof: It follows from Proposition 2 that the stability–regularity holds iff every real zero of Q on $(-2, 2)$ has an *even* multiplicity. This means that, if Q has a zero on $(-2, 2)$, it must be an *extremum*. Since any zero at ± 2 is necessarily even (see (44)), one sees that the stability—regularity is equivalent to

$$\max_{\omega \in [-2,2]} Q(\omega) \leq 0 \quad \text{or} \quad \min_{\omega \in [-2,2]} Q(\omega) \geq 0. \tag{59}$$

One can easily show that (59) is equivalent to

$$\max_{\omega \in [-2,2]} a_m Q(\omega) \leq 0 \quad \text{or} \quad \min_{\omega \in [-2,2]} a_m Q(\omega) \geq 0. \tag{60}$$

We claim that the second inequality in (60) is always violated under our standing assumptions: $a_0 < 0$, $a_m \neq 0$. In order to show this, consider (see (45))

$$a_m Q(\omega) = a_0 + \sum_{p=1}^{m} a_p \left(\lambda^p + \lambda^{-p}\right) \tag{61}$$

where ω and λ are related via (44). Since we are interested in ω on $[-2, 2]$, λ is represented as

$$\lambda = e^{j\theta}, \qquad \theta \in [0, \pi].$$

Hence

$$\begin{aligned} \sum_{p=1}^{m} a_p \left(\lambda^p + \lambda^{-p}\right) &= \sum_{p=1}^{m} a_p \left(e^{jp\theta} + e^{-jp\theta}\right) \\ &= 2 \sum_{p=1}^{m} a_p \cos(p\theta). \end{aligned} \tag{62}$$

It follows from

$$\int_0^{\pi} 2 \sum_{p=1}^{m} a_p \cos(p\theta)\, d\theta = 0 \tag{63}$$

that (62) is either identically zero or changes sign on $[0, \pi]$. Since $a_m \neq 0$, the first possibility is excluded. Therefore, if $a_0 < 0$, then (61) cannot be always positive on $[-2, 2]$; hence the second inequality in (60) is always violated. □

Proposition 5: A neural network described by (11) is spatially stable *if and only if*

$$\sigma_+(a_0, a_1, \cdots, a_m) < 0. \tag{64}$$

Proof: It follows from Proposition 3 that the spatial stability is equivalent to the fact that Q has no real zero on $[-2, 2]$, which, in turn, is equivalent to

$$\max_{\omega \in [-2,2]} a_m Q(\omega) < 0 \quad \text{or} \quad \min_{\omega \in [-2,2]} a_m Q(\omega) > 0. \tag{65}$$

By using the argument used in the proof of Proposition 4, one sees that the second inequality in (65) is always violated. □

The following fact gives upper and lower bounds for eigenvalues of the temporal dynamics $\boldsymbol{A}$.

Proposition 6:

i) Any eigenvalue μ of the temporal dynamics $\boldsymbol{A}$ for any n satisfies the following bounds:

$$\sigma_-(a_0, a_1, \cdots, a_m) < \mu < \sigma_+(a_0, a_1, \cdots, a_m). \tag{66}$$

ii) The bounds (66) are *optimal* in the sense that if σ_+^* (resp. σ_-^*) is any number which satisfies

$$\begin{aligned} &\sigma_+^* < \sigma_+(a_0, a_1, \cdots, a_m) \\ &\left(\text{resp. } \sigma_-(a_0, a_1, \cdots, a_m) < \sigma_-^*\right) \end{aligned}$$

then there is an eigenvalue μ of $\boldsymbol{A}$ for some n such that

$$\sigma_+^* < \mu \qquad \left(\text{resp. } \mu < \sigma_-^*\right).$$

Proof: See Appendix II.

Remark 10: Note that (58) is a weak inequality, i.e., equality is allowed, while (66) does not allow the equality. This is exactly what it should be. If, for instance $\sigma_+(a_0, a_1, \cdots, a_m) = 0$, then Proposition 4 tells us that the network is temporally

stable and hence that all the eigenvalues of $\boldsymbol{A}$ are strictly negative, which is what (66) says.

We would like to emphasize the *if and only if* nature of Proposition 4 as well as Proposition 5 and the *optimality* of Proposition 6, which indicate that $\sigma_+(a_0, a_1, \cdots, a_m)$ and $\sigma_-(a_0, a_1, \cdots, a_m)$ are crucial to the stability issues of our interest. The above propositions, however, would not be very useful unless one could compute explicit formulas for $\sigma_+(a_0, a_1, \cdots, a_m)$ and $\sigma_-(a_0, a_1, \cdots, a_m)$. In the following, we will compute these functions for $m \leq 3$.

B. $m = 2$

We begin with $m = 2$, which motivated the present study.

Proposition 7: When $m = 2$, the stability indicator functions are given by

$$\sigma_+(g_0, g_1, g_2) = \begin{cases} -g_0 - 2g_1 + 2|g_1| & \text{when } g_2 > 0 \text{ or } g_2 < 0 \text{ and } |g_1/g_2| \geq 4 \\ -g_0 - 2g_1 - 4g_2 - g_1^2/4g_2 & \text{when } g_2 < 0 \text{ and } |g_1/g_2| \leq 4 \end{cases}$$

$$\sigma_-(g_0, g_1, g_2) = \begin{cases} -g_0 - 2g_1 - 2|g_1| & \text{when } g_2 < 0 \text{ or } g_2 > 0 \text{ and } |g_1/g_2| \geq 4 \\ -g_0 - 2g_1 - 4g_2 - g_1^2/4g_2 & \text{when } g_2 > 0 \text{ and } |g_1/g_2| \leq 4. \end{cases} \tag{67}$$

Proof: See Appendix III.

Example 3: With Propositions 4–7 at hand, we can now check Fig. 3 and Fig. 4 theoretically. In Figs. 3 and 4, $1/g_0 = 200\ \text{k}\Omega$ and $1/g_1 = 5\ \text{k}\Omega$ are fixed while g_2 is varied: (a) $1/g_2 = -20\ \text{k}\Omega$; (b) $1/g_2 = -18\ \text{k}\Omega$; and (c) $1/g_2 = -17\ \text{k}\Omega$. In order to check (a), note that $|g_1/g_2| = 4$; hence (67) gives

$$\sigma_+(g_0, g_1, g_2) = -g_0 < 0.$$

Propositions 4 and 5 guarantee the temporal as well as the spatial stability. For (b), $|g_1/g_2| = 18/5 < 4$ and (67) reads

$$\begin{aligned} \sigma_+(g_0, g_1, g_2) &= -g_0 - 2g_1 - 4g_2 - g_1^2/4g_2 \\ &= (-1/200 - 2/5 + 4/18 + 18/100) \\ &\quad \times 10^{-3} < 0 \end{aligned}$$

which checks Fig. 3(b) and Fig. 4(b). Finally, for (c),

$$\begin{aligned} \sigma_+(g_0, g_1, g_2) &= (-1/200 - 2/5 + 4/17 + 17/100) \\ &\quad \times 10^{-3} > 0 \end{aligned}$$

and hence the network is temporally and spatially unstable, which checks Fig. 3(c) and Fig. 4(c).

Example 4: For the Gaussian-like convolver [1]

$$g_1 > 0, \qquad g_2 < 0, \qquad g_1 = 4|g_2|. \tag{68}$$

(Appendix IV gives a simple explanation for this choice of conductance values.) Propositions 4 and 7 tell us that the stability–regularity is equivalent to

$$\sigma_+(g_0, g_1, g_2) = -g_0 \leq 0,$$

i.e., passivity of g_0. Furthermore, Proposition 5 says that the network is spatially stable iff

$$\sigma_+(g_0, g_1, g_2) = -g_0 < 0,$$

i.e., iff g_0 is strictly passive. Thus g_0 can be safely varied over any range as long as it is positive.

Remark 11:

i) Even when g_1 as well as g_2 is negative, a network can satisfy the stability–regularity or/and the spatial stability condition provided that g_0 is "sufficiently" passive because

$$\sigma_+(g_0, g_1, g_2) = \begin{cases} -g_0 + 4|g_1| & \text{when } |g_1/g_2| \geq 4 \\ -g_0 + 2|g_1| + 4|g_2| + g_1^2/4|g_2| & \text{when } |g_1/g_2| \leq 4. \end{cases}$$

ii) If $g_2 > 0$, then

$$\sigma_+(g_0, g_1, g_2) = \begin{cases} -g_0 & \text{when } g_1 \geq 0 \\ -g_0 + 4|g_1| & \text{when } g_1 \leq 0. \end{cases}$$

iii) Since Q is quadratic, conditions (ii) and (iii) of Proposition 2 are sharpened, respectively to the following:

(ii)′ $\boldsymbol{F}$ has no simple nonreal eigenvalue on the unit circle.

(iii)′ Q has no real zero on $(-2, 2)$.

It follows from Proposition 4 (resp. Proposition 6) that the set of parameter values (g_0, g_1, g_2) for which stability–regularity and the spatial stability hold are given, respectively, by

$$\text{SR} = \{(g_0, g_1, g_2) | \sigma_+(g_0, g_1, g_2) \leq 0,\ g_0 + 2g_1 + 2g_2 > 0\} \tag{69}$$

$$\text{SS} = \{(g_0, g_1, g_2) | \sigma_+(g_0, g_1, g_2) < 0,\ g_0 + 2g_1 + 2g_2 > 0\}. \tag{70}$$

We will now give a fact which, as its by-product, explains why our numerical experiments suggested SR = SS, which is untrue. Let

$$G = \{(g_0, g_1, g_2) | g_2 < 0\}$$

on which our numerical experiments were performed.

Proposition 8:

i) $\text{meas}[\text{SS} \cap G] > 0$

ii) $\text{meas}[(\text{SR} - \text{SS}) \cap G] = 0$

where meas[·] denotes the Lebesgue measure on $\mathbb{R}^3$.

Proof: It follows from (67) that SS $\cap$ G contains an open set of $\mathbb{R}^3$ and hence it is of positive Lebesgue measure. Since SR $\supset$ SS, the set difference SR − SS makes sense, and

meas[SR $\cap$ G] $>$ 0. The set (SR $-$ SS) $\cap$ G is a subset of SR $\cap$ G such that

$$\sigma_+(g_0, g_1, g_2) = 0. \tag{71}$$

Since the gradient of $\sigma_+(g_0, g_1, g_2)$ on (SR $-$ SS) $\cap$ G is given by

$$D\sigma_+(g_0, g_1, g_2) = \begin{cases} (-1, 0, 0) & \text{when } g_1 > 0,\ |g_1/g_2| \geq 4 \\ (-1, -4, 0) & \text{when } g_1 < 0,\ |g_1/g_2| \geq 4 \\ (-1, -2 - g_1/2g_2, -4 + g_1^2/4g_2^2) & \text{when } |g_1/g_2| \geq 4 \end{cases}$$

and since this is nonvanishing, (71) forces (g_0, g_1, g_2) to lie in a Lebesgue measure zero subset [20, lemma 4]. □

Remark 12: This proposition explains why our experiments suggested SR = SS for a Lebesgue measure zero subset is "hard to hit."

C. $m = 1$

Neural networks with $m = 1$ are used in an extensive manner [6]–[8]. Although those networks contain only positive conductances $(g_0, g_1 > 0)$, it would be worth clarifying the temporal as well as the spatial stability issues when $g_1 < 0$. We will state the result without proof because the proof is much simpler than in the $m = 2$ case.

Proposition 9: When $m = 1$, the stability indicators are given by

$$\sigma_+(g_0, g_1) = -g_0 - 2g_1 + 2|g_1|$$
$$\sigma_-(g_0, g_1) = -g_0 - 2g_1 - 2|g_1|.$$

Example 5: When $g_0 > 0$ but $g_1 < 0$, the stability issues are nontrivial. The network is temporally (resp. spatially) stable iff

$$-g_0 + 4|g_1| \leq 0 \qquad (\text{resp.} - g_0 + 4|g_1| < 0).$$

In Example 2, $1/g_0 = 100$ kΩ, $1/g_1 = -800$ kΩ, and $\sigma_+(g_0, g_1) = (-1/100 + 4/800) \times 10^{-3} < 0$ and the network is temporally as well as spatially stable which checks Fig. 9(a).

Remark 13: One can show for this case also that the set of (g_0, g_1) values on which the temporal stability holds, and yet the spatial stability fails, is of measure zero,

D. $m = 3$

As was remarked earlier, neurochips with $m \leq 2$ have already been designed and fabricated. Although no result has been reported on chips with $m = 3$, we conjecture that this architecture might be suitable for noncausual IIR implementations of interesting image processing filters.

We saw in subsection III-B and Appendix III that the case $m = 2$ is already sufficiently complicated to require a careful analysis. Naturally, the case $m = 3$ is even more involved and we need to prepare several notations. First note that, when $m = 3$,

$$Q(\omega) = \left(\frac{a_0}{a_3} - 2\frac{a_2}{a_3}\right) + \left(\frac{a_1}{a_3} - 3\right)\omega + \frac{a_2}{a_3}\omega^2 + \omega^3 \tag{72}$$

and that

$$a_0 = -(g_0 + 2g_1 + 2g_2 + 2g_3), \qquad a_1 = g_1, \qquad a_2 = g_2, \qquad a_3 = g_3. \tag{73}$$

The zeros of the derivative $dQ/d\omega$ are

$$\xi_\pm = \left(-\frac{a_2}{a_3} \pm \sqrt{D}\right)/3 = \left(-\frac{g_2}{g_3} \pm \sqrt{D}\right)/3 \tag{74}$$

where

$$D = \left(\frac{a_2}{a_3}\right)^2 - 3\left(\frac{a_1}{a_3}\right) + 9 = \left(\frac{g_2}{g_3}\right)^2 - 3\left(\frac{g_1}{g_3}\right) + 9. \tag{75}$$

Using (74), one has

$$\begin{aligned} Q(\xi_\pm) &= 3\xi_\pm\left[-\frac{2}{9}\left(\frac{a_2}{a_3}\right)^2 + \frac{2}{3}\left(\frac{a_1}{a_3}\right) - 2\right] \\ &\quad - \frac{1}{9}\frac{a_2}{a_3}\frac{a_1}{a_3} - \frac{5}{3}\frac{a_2}{a_3} + \frac{a_0}{a_3} \\ &= 3\xi_\pm\left[-\frac{2}{9}\left(\frac{g_2}{g_3}\right)^2 + \frac{2}{3}\left(\frac{g_1}{g_3}\right) - 2\right] - \frac{1}{9}\frac{g_2 g_1}{g_3^2} \\ &\quad - \frac{g_0}{g_3} - \frac{2g_1}{g_3} - \frac{11}{3}\frac{g_2}{g_3} - 2. \end{aligned} \tag{76}$$

Note that

$$Q(2) = \frac{a_0}{a_3} + 2\frac{a_1}{a_3} + 2\frac{a_2}{a_3} + 2 = -\frac{g_0}{g_3}$$
$$Q(-2) = \frac{a_0}{a_3} - 2\frac{a_1}{a_3} + 2\frac{a_2}{a_3} - 2 = -\frac{g_0}{g_3} - 4\frac{g_1}{g_3} - 4$$

and define

$$f_+ := a_3 Q(2) = -g_0 \tag{77}$$
$$f_- := a_3 Q(-2) = -g_0 - 4g_1 - 4g_3 \tag{78}$$

$$\begin{aligned} h_\pm &:= a_3 Q(\xi_\pm) \\ &= 3\xi_\pm\left[-\frac{2}{9}\frac{g_2^2}{g_3} + \frac{2}{3}g_1 - 2g_3\right] - \frac{1}{9}\frac{g_2 g_1}{g_3} \\ &\quad - g_0 - 2g_1 - \frac{11}{3}g_2 - 2g_3. \end{aligned} \tag{79}$$

Proposition 10: When $m = 3$, the stability indicator functions are given by

$$\sigma_+(g_0,g_1,g_2,g_3)=\begin{cases} f_+ & \text{when } g_3>0,\ D\le 0 \quad \text{or} \quad g_3>0,\ D>0,\ \xi_-<\xi_+\le -2 \\ & \text{or} \quad g_3>0,\ D>0,\ 2\le\xi_-<\xi_+ \\ & \text{or} \quad g_3<0,\ D>0,\ \xi_-\le -2,\ 2\le\xi_+ \\ f_- & \text{when } g_3>0,\ D>0,\ \xi_-\le -2,\ 2\le\xi_+ \\ & \text{or} \quad g_3<0,\ D\le 0 \quad \text{or} \quad g_3<0,\ D>0,\ \xi_-<\xi_+\le -2 \\ & \text{or} \quad g_3<0,\ D>0,\ 2\le\ \xi_-<\xi_+ \\ \max[f_+,f_-] & \text{when } g_3>0,\ \xi_-\le -2\le\xi_+\le 2 \\ & \text{or} \quad g_3<0,\ -2\le\xi_-\le 2\le\xi_+ \\ h_+ & \text{when } g_3>0,\ \xi_-\le -2\le\xi_+\le 2 \\ h_- & \text{when } g_3>0,\ -2\le\xi_-\le 2\le\xi_+ \\ \max[f_+,h_-] & \text{when } g_3>0,\ -2\le\xi_-<\xi_+\le 2 \\ \max[f_-,h_+] & \text{when } g_3<0,\ -2\le\xi_-\le\xi_+\le 2 \end{cases}$$

$$\sigma_-(g_0,g_1,g_2,g_3)=\begin{cases} f_+ & \text{when } g_3>0,\ D>0,\ \xi_-\le -2,\ 2\le\xi_+ \quad \text{or} \quad g_3<0,\ D\le 0 \\ & \text{or} \quad g_3<0,\ D>0,\ \xi_-<\xi_+\le -2 \\ & \text{or} \quad g_3<0,\ D>0,\ 2\le\xi_-<\xi_+ \\ f_- & \text{when } g_3>0,\ D\le 0, \quad \text{or} \quad g_3>0,\ D>0,\ \xi_-<\xi_+\le -2 \\ & \text{or} \quad g_3>0,\ D>0,\ 2\le\xi_-<\xi_+ \\ & \text{or} \quad g_3<0, D>0, \xi_-<-2, 2\le\xi_+ \\ \min[f_+,f_-] & \text{when } g_3<0,\ -2\le\xi_-\le 2\le\xi_+ \\ & \text{or} \quad g_3>0,\ \xi_-\le -2\le\xi_+\le 2 \\ h_+ & \text{when } g_3>0,\ -2\le\xi_-\le 2\le\xi_+ \\ h_- & \text{when } g_3<0,\ \xi_-\le -2\le\xi_+\le 2 \\ \min[f_+,h_-] & \text{when } g_3<0,\ -2\le\xi_-\le\xi_+\le 2 \\ \min[f_-,h_+] & \text{when } g_3>0,\ -2\le\xi_-<\xi_+\le 2. \end{cases}$$

Proof: See Appendix V.

IV. Transients

This section analyzes the capacitance matrix $\boldsymbol{B}$ in (4) using the method used for analyzing $\boldsymbol{A}$. As a by-product, an estimate will be obtained of the "processing speed" of neuro chips.

It follows from (4) that the capacitance matrix $\boldsymbol{B}$ has exactly the same structure as that of $\boldsymbol{A}$. Therefore, one can derive conditions under which $\boldsymbol{B}$ is *positive* definite and bounds on its eigenvalues. Let

$$P_B(\lambda) := \lambda^m\left[\frac{b_0}{b_m}+\sum_{p=1}^{m}\frac{b_p}{b_m}\left(\lambda^p+\lambda^{-p}\right)\right]$$

$$Q_B(\omega) := \frac{b_0}{b_m}+\sum_{p=1}^{m}\frac{b_p}{b_m}\left(\lambda^p+\lambda^{-p}\right)$$

where $b_0,\cdots,b_m$ are as in (4) while ω and λ are as in (44). Define

$$\eta_+(b_0,b_1,\cdots,b_m) := \max_{\omega\in[-2,2]} b_m Q_B(\omega) \tag{80}$$

$$\eta_-(b_0,b_1,\cdots,b_m) := \min_{\omega\in[-2,2]} b_m Q_B(\omega) \tag{81}$$

The following fact can be proved by an argument similar to that used for the negative definiteness of $\boldsymbol{A}$.

Proposition 11: Replace (ii) of the standing assumptions (subsection II-C) by

$$b_0>0, \qquad b_m\neq 0. \tag{82}$$

i) The following conditions are equivalent:

a) $\boldsymbol{B}$ is positive definite for all n.

b) Every nonreal zero λ_c of $P_B(\lambda)$ with $|\lambda_c|=1$ has an even multiplicity.

c) Every real zero ω_R of $Q_B(\omega)$ with $|\omega_R|<2$ has an even multiplicity.

d)

$$\eta_-(b_0,b_1,\cdots,b_m)\ge 0 \tag{83}$$

ii) Any eigenvalue ν of $\boldsymbol{B}$ for any n, satisfies

$$\eta_-(b_0,b_1,\cdots,b_m)<\nu<\eta_+(b_0,b_1,\cdots,b_m) \tag{84}$$

and the bounds are optimal.

Corollary 1: Assume (82) and consider the temporal dynamics (5) with $\boldsymbol{v}(0)=\boldsymbol{0}$. If (58) and (83) are satisfied, then the solution $\boldsymbol{v}(t)$ of (5) satisfies the following bounds:

$$\frac{\eta_-}{\sigma_-}\left[\exp\left(\frac{\sigma_-}{\eta_-}t\right)-1\right]\left\|\boldsymbol{B}^{-1}\boldsymbol{u}\right\|\le\|\boldsymbol{v}(t)\| \le\frac{\eta_+}{\sigma_+}\left[\exp\left(\frac{\sigma_+}{\eta_+}t\right)-1\right]\left\|\boldsymbol{B}^{-1}\boldsymbol{u}\right\| \tag{85}$$

Proof: See Appendix VI.

Remark 14:

i) The result tells us how fast/slow a step response of (5) grows. Although there is no precise concept of the

time constant RC for (5) ($\dim \boldsymbol{v} \gg 1$), (85) can be interpreted as

$$-\frac{\eta_-}{\sigma_-} \leq \text{"time constant"} \leq -\frac{\eta_+}{\sigma_+}. \tag{86}$$

ii) Let us compute the upper bound in (86) for $m = 2$. It is not difficult to show that

$$\eta_+(c_0, c_1, c_2) = \begin{cases} c_0 + 2c_1 + 2|c_1| & \text{when } c_2 < 0 \text{ or } c_2 > 0 \text{ and } |c_1/c_2| \geq 4 \\ c_0 + 2c_1 + 4c_2 + c_1^2/4c_2 & \text{when } c_2 > 0 \text{ and } |c_1/c_2| \leq 4. \end{cases}$$

If $g_0, g_1, c_0, c_1, c_2 > 0$, then it follows from (67) and the above formula that

$$-\frac{\eta_+}{\sigma_+} = -\frac{\eta_+}{g_0} = \begin{cases} (c_0 + 4c_1)/g_0 & \text{when } |c_1/c_2| \geq 4 \\ (c_0 + 2c_1 + 4c_2 + c_1^2/4c_2)/g_0 & \text{when } |c_1/c_2| \leq 4. \end{cases}$$

Since it is difficult to estimate parasitic capacitances accurately, this is as much as one can tell from the corollary.

V. Concluding Remarks

(i) We would like to call the reader's attention to the fact that the spatial dynamics of the class of neural networks discussed here are *zero phase* and yet IIR. More specifically, consider the transfer function of the spatial dynamics in the frequency domain:

$$1/H(z) = 1/\left[a_m z^{-m} P_F(z)\right]$$

where P_F is the characteristic polynomial defined by (41). Then

$$H\left(e^{j\omega}\right) = a_0 + \sum_{p=1}^{m} 2a_p \cos(p\omega)$$

which is *real*. Obviously, a zero-phase filter is ideal in signal processing, for if the phase does not behave properly, the signal would be distorted. It is known [21] that a stable linear-phase IIR *cannot* be realized by a *causal* system (linear-phase meaning here that the phase is linear in ω). Thus the spatial dynamics (11) are a zero-phase noncausal IIR filter. The results reported here establish conditions under which those noncausal IIR filters are temporally and/or spatially stable.

(ii) Using an argument used in the proof of Lemma A2, one can show that if $a_0 > 0$, i.e., if the diagonal element of $\boldsymbol{A}$ is positive, then $\boldsymbol{A}$ is *positive* definite iff the spatial dynamics is regular. Since the definition of spatial stability (Definition 2) is the hyperbolicity of $\boldsymbol{F}$, the spatial dynamics can be stable even when $a_0 > 0$. Thus, the spatial regularity or stability can be satisfied even when $\boldsymbol{A}$ is positive definite, while temporal stability is certainly violated if $\boldsymbol{A}$ is positive definite. This *asymmetry* is due to the fact that the spatial dynamics is noncausal whereas the temporal dynamics is causal.

(iii) Recall Proposition 8, which states that, for $m = 2$, the temporal stability coincides with the spatial stability except for a measure zero subset of $\mathbb{R}^3$.

Conjecture: Proposition 8 will be true for a general m.

(iv) The following is a list of possible future research projects:

a) Generalizations to nonlinear cases, e.g., the chip reported in [11]. While the temporal stability results can be established under reasonable conditions, the spatial stability results may not be easy to obtain because the spatial dynamics are not only nonlinear but also nonautonomous with respect to node number k. More specifically, let

$$\boldsymbol{B}\frac{d\boldsymbol{v}}{dt} = \boldsymbol{G}(\boldsymbol{v}) + \boldsymbol{u} \tag{87}$$

be the temporal dynamics where $\boldsymbol{G} : \mathbb{R}^n \to \mathbb{R}^n$. Let $\boldsymbol{v}$ be an equilibrium of (87) and suppose that

$$\boldsymbol{x}_{k+1} = \boldsymbol{F}(\boldsymbol{x}_k) + \boldsymbol{y}_k \tag{88}$$

represents the spatial dynamics in the sense of (11), where $\boldsymbol{F} : \mathbb{R}^{2m} \to \mathbb{R}^{2m}$. Therefore, the spatial stability means the stability of the trajectory (88), which is not necessarily a fixed point of $\boldsymbol{F}$. Furthermore, if the conductances are nonlinear, the temporal dynamics are not necessarily of the popular form

$$\boldsymbol{B}\frac{d\boldsymbol{v}}{dt} = -\frac{1}{R}\boldsymbol{v} + \boldsymbol{T}\boldsymbol{G}(v) + \boldsymbol{u}$$

where $\boldsymbol{T}$ is symmetric, $\boldsymbol{G} = \left(G^1, \cdots, G^n\right)$, and G^i, $i = 1, \cdots, n$, is sigmoidal.

b) Generalization to two-dimensional array cases.

c) IIR implementations and associated stability of other interesting filters, e.g., oriented receptive field filters [4] and Gabor filters [5].

d) It could be interesting to investigate the relationship, if any, with the stability results for neural field equations [22], [23].

Appendix I
Proof of Theorem 1

Throughout this appendix, the center eigenspace E^c is empty. Hence any vector $\boldsymbol{x} \in E$ can be written as $\boldsymbol{x} = \boldsymbol{x}^u + \boldsymbol{x}^s$, $\boldsymbol{x}^u \in E^u$, $\boldsymbol{x}^s \in E^s$. Proposition A1 says that a slight enlargement of E^u does not destroy the property $E^u \cap T_+ = \{\boldsymbol{0}\}$; i.e., the intersection between E^u and T_+ is the singleton set $\{\boldsymbol{0}\}$ and that the same is true for E^s and T_-. Proposition A2 says that $\boldsymbol{x}_1$ (resp. $\boldsymbol{x}_0$) approaches E^u (resp. E^s) as $K \to +\infty$. Lemma A1 tells us that $\boldsymbol{x}_1$ (resp. $\boldsymbol{x}_0$) approaches $\overline{\boldsymbol{x}}_1$ (resp. $\overline{\boldsymbol{x}}_0$) as $K \to +\infty$.

Proposition A1: There are positive numbers α_+ and α_- such that

$$\begin{aligned} \Lambda_{\alpha+}(E^u) \cap T_+ &= \{\boldsymbol{0}\} \\ \Lambda_{\alpha-}(E^s) \cap T_- &= \{\boldsymbol{0}\} \end{aligned} \tag{A1}$$

where $\Lambda_{\alpha+}(E^u)$ and $\Lambda_{\alpha-}(E^s)$ are the α_+ sector of E^u and the α_- sector of E^s, respectively (Fig. 13):

$$\begin{aligned} \Lambda_{\alpha+}(E^u) &:= \{(\boldsymbol{z}^u, \boldsymbol{z}^s) \in E^u \oplus E^s \mid \|\boldsymbol{z}^s\| < \alpha_+ \|\boldsymbol{z}^u\|\} \\ \Lambda_{\alpha-}(E^s) &:= \{(\boldsymbol{z}^u, \boldsymbol{z}^s) \in E^u \oplus E^s \mid \|\boldsymbol{z}^u\| < \alpha_- \|\boldsymbol{z}^s\|\}. \end{aligned}$$

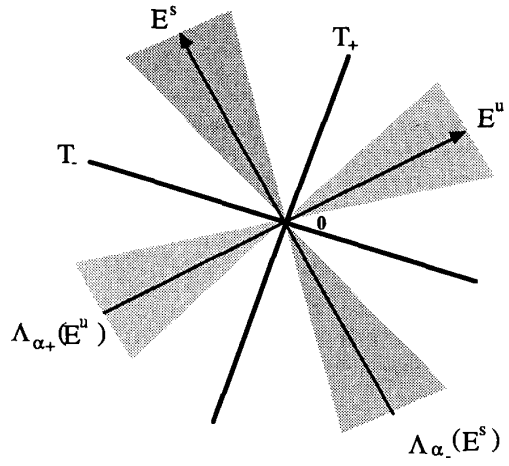

Fig. 13. The α_+ section of E^u and the α_- section of E^s.

Proof: Since $T_+ \oplus E^u = E^s \oplus E^u$, there is a unique linear map $\tau_+^u : E^u \to E^s$ such that

$$T_+ = \left\{ \left(z^u, \tau_+^u z^u \right) \in E^u \oplus E^s \mid z^u \in E^u \right\}.$$

Since $T_+ \cap E^u = \{0\}$, the map τ_+^u is nonsingular; hence

$$\alpha_+ := \inf \left\{ \left\| \tau_+^u z^u \right\| \mid z^u \in E^u, \|z^u\| = 1 \right\}$$

is positive. Clearly (A1) is satisfied. A similar argument is valid for $\Lambda_{\alpha-}(E^s)$.

Proposition A2: If $\{x_k\}_{-K}^{+K}$ is a solution for (T_+, T_-, K), then

$$\|x_1^u\| \le \alpha_+^{-1} \lambda_\#^{-2(K-1)} \|x_1^s\|$$
$$\|x_0^s\| \le \alpha_-^{-1} \lambda_\#^{-2K} \|x_0^u\|$$

where $\lambda_\#$ is defined by (25).

Proof: Since $x_K \in T_+$, one has $x_K \notin \Lambda_{\alpha+}(E^u)/\{0\}$ so that $\|x_K^s\| \ge \alpha_+ \|x_K^u\|$. It follows from $\|x_{k+1}^s\| = \|F x_k^s\| \le \lambda_\#^{-1} \|x_k^s\|$ that $\|x_K^s\| \le \lambda_\#^{-(K-1)} \|x_1^s\|$. Therefore

$$\|x_K^u\| \le \alpha_+^{-1} \|x_K^s\| \le \alpha_+^{-1} \lambda_\#^{-(K-1)} \|x_1^s\|,$$

hence

$$\|x_1^u\| \le \alpha_+^{-1} \lambda_\#^{-2(K-1)} \|x_1^s\|. \tag{96}$$

The other inequality can be derived in a similar manner. □

Now let $\overline{\Lambda}_\varepsilon(E^u)$ and $\overline{\Lambda}_\varepsilon(E^s)$ denote the *closed* ε sectors of E^u and E^s respectively:

$$\overline{\Lambda}_\varepsilon(E^u) := \{(z^u, z^s) \in E^u \oplus E^s \mid \|z^s\| \le \varepsilon \|z^u\|\}$$
$$\overline{\Lambda}_\varepsilon(E^s) := \{(z^u, z^s) \in E^u \oplus E^s \mid \|z^u\| \le \varepsilon \|z^s\|\}.$$

Then Proposition A2 says that a solution $\{x_k\}_{-K}^{+K}$ for (T_+, T_-, K) satisfies

$$x_0 \in \overline{\Lambda}\varepsilon_1(E^u), \qquad x_1 \in \overline{\Lambda}\varepsilon_2(E^s), \qquad x_1 = F^d x_0 + y_0 \tag{A2}$$

where

$$\varepsilon_1 = \alpha_-^{-1} \lambda_\#^{-2K} \qquad \varepsilon_2 = \alpha_+^{-1} \lambda_\#^{-2(K-1)}. \tag{A3}$$

Lemma A1: Let $\varepsilon_1, \varepsilon_2 > 0$ satisfy

$$\max\left[\varepsilon_1 (1-\varepsilon_1)^{-1}, \varepsilon_2 (1-\varepsilon_2)^{-1}, \varepsilon_1, \varepsilon_2 \right] \le 1/4 \tag{A4}$$

and let

$$r = 2\left(\|\overline{x}_1\| + \left\| F^d \overline{x}_0 \right\| \right). \tag{A5}$$

If

$$z \in \left(\overline{\Lambda}\varepsilon_1(E^u) + y_0 \right) \cap \overline{\Lambda}\varepsilon_2(E^s), \tag{A6}$$

then

$$z = w + y_0 \qquad w \in \overline{\Lambda}\varepsilon_1(E^u) \tag{A7}$$

and

$$\|z\| + \|w\| \le r \tag{A8}$$
$$\|z - \overline{x}_1\| \le \varepsilon_1 (1-\varepsilon_1)^{-1} \|w\| + \varepsilon_2 (1-\varepsilon_2)^{-1} \|z\| \tag{A9}$$
$$\left\| w - F^d \overline{x}_0 \right\| \le \varepsilon_1 (1-\varepsilon_1)^{-1} \|w\| + \varepsilon_2 (1-\varepsilon_2)^{-1} \|z\|. \tag{A10}$$

Proof: If (A6) holds, $z \in \overline{\Lambda}\varepsilon_2(E^s)$ implies

$$z = z^u + z^s, \qquad z^u \in E^u, \qquad z^s \in E^s,$$
$$\text{and} \quad \|z^u\| \le \varepsilon_2 \|z^s\|$$

which, in turn, implies

$$\|z^s\| = \|z - z^u\| \le \|z\| + \|z^u\| \le \|z\| + \varepsilon_2 \|z_s\|.$$

Therefore

$$\|z^s\| \le (1-\varepsilon_2)^{-1} \|z\| \tag{A11}$$

and hence

$$\|z^u\| \le \varepsilon_2 (1-\varepsilon_2)^{-1} \|z\|. \tag{A12}$$

Since $z \in \overline{\Lambda}\varepsilon_1(E^u) + y_0$ ((A6)), one has

$$z - y_0 = w^u + w^s, \qquad w^u \in E^u, \qquad w^s \in E^s$$
$$\|w^s\| \le \varepsilon_1 \|w^u\| \tag{A13}$$

from which it follows that

$$\|w^s\| \le \varepsilon_1 (1-\varepsilon_1)^{-1} \|w\|. \tag{A14}$$

Let us rewrite the equality (see (A13))

$$z^u + z^s = w^u + w^s + y_0$$

and

$$z^s - w^s = w^u - z^u + y_0.$$

Then the uniqueness of the stable free-boundary solution (Proposition 1) implies that there is a unique pair $(\overline{x}_1, \overline{x}_0)$ satisfying (see (24))

$$\overline{x}_1 = z^s - w^s \qquad F^d \overline{x}_0 = w^u - z^u. \tag{A15}$$

It follows from (A11), (A12), (A14), and (A15) that

$$\begin{aligned}\|z-\bar{x}_1\| &= \|z^u+z^s-(z^s-w^s)\| \\ &= \|z^u+w^s\| \le \|z^u\|+\|w^s\| \\ &\le \varepsilon_1(1-\varepsilon_1)^{-1}\|w\|+\varepsilon_2(1-\varepsilon_2)^{-1}\|z\|\end{aligned}$$

which proves (A9). Similarly

$$\begin{aligned}\left\|w-F^d\bar{x}_0\right\| &= \|w^u+w^s-(w^u-z^u)\| \\ &\le \|w^s\|+\|z^u\| \\ &= \varepsilon_1(1-\varepsilon_1)^{-1}\|w\|+\varepsilon_2(1-\varepsilon_2)^{-1}\|z\|\end{aligned}$$

which proves (A10). In order to show (A8), observe that

$$\|z\|-\|\bar{x}_1\| \le \|z-\bar{x}_1\|$$

and

$$\|w\|-\left\|F^d\bar{x}_0\right\| \le \left\|w-F^d\bar{x}_0\right\|$$

imply

$$\begin{aligned}\|z\| &\le \|\bar{x}_1\|+\|z-\bar{x}_1\| \\ &\le \|\bar{x}_1\|+\varepsilon_1(1-\varepsilon_1)^{-1}\|w\|+\varepsilon_2(1-\varepsilon_2)^{-1}\|z\|\end{aligned} \tag{A16}$$

and

$$\begin{aligned}\|w\| &\le \left\|F^d\bar{x}_0\right\|+\left\|w-F^d\bar{x}_0\right\| \\ &\le \left\|F^d\bar{x}_0\right\|+\varepsilon_1(1-\varepsilon_1)^{-1}\|w\|+\varepsilon_2(1-\varepsilon_2)^{-1}\|z\|.\end{aligned} \tag{A17}$$

Adding (A16) and (A17), one has

$$\begin{aligned}\|z\|+\|w\| &\le \|\bar{x}_1\|+\left\|F^d\bar{x}_0\right\|+2\varepsilon_1(1-\varepsilon_1)^{-1}\|w\| \\ &\quad +2\varepsilon_2(1-\varepsilon_2)^{-1}\|z\| \\ &\le \|\bar{x}_1\|+\left\|F^d\bar{x}_0\right\| \\ &\quad +2\max\left[\varepsilon_1(1-\varepsilon_1)^{-1},\varepsilon_2(1-\varepsilon_2)^{-1}\right] \\ &\quad \cdot(\|w\|+\|z\|) \\ &\le \|\bar{x}_1\|+\left\|F^d\bar{x}_0\right\|+1/2(\|w\|+\|z\|)\end{aligned}$$

where (A4) was used. This inequality together with (A5) implies

$$\|z\|+\|w\| \le 2\left(\|\bar{x}_1\|+\left\|F^d\bar{x}_0\right\|\right)=r. \qquad \square$$

Completion of the Proof: It follows from Proposition A2 that (A4) is satisfied for K sufficiently large. Since F^d expands the vectors in E^u while it contracts the vectors in E^s, one sees that

$$x_0 \in \bar{\Lambda}\varepsilon_1(E^u) \text{ implies } F^d x_0 \in \bar{\Lambda}\varepsilon_1(E^u).$$

Therefore, one can take

$$x_1 = F^d x_0 + y_0$$

as the z in (A7) of Lemma A1, and (A8) reads

$$\|x_1\|+\left\|F^d x_0\right\| \le r$$

and

$$\|x_1^s\| \le \|x_1\| \le r. \tag{A18}$$

Since $x_K = F^{K-1}x_1$, (A18) implies

$$\|x_K\| \le \lambda_\#^{-(K-1)} r. \tag{A19}$$

In order to estimate $\|x_k^u\|$, let

$$\tau_+^s : E^s \to E^u$$

be the linear map such that

$$T_+ = \left\{\left(\tau_+^s z^s, z^s\right) \in E^u \oplus E^s | z^s \in E^s\right\}. \tag{A20}$$

This map is well defined and is unique because of (34). It follows from (A20) that

$$\begin{aligned}\|x_K\| = \left\|\left(\tau_+^s x_K^s, x_K^s\right)\right\| &\le \left(\left\|\tau_+^s\right\|+1\right)\|x_K^s\| \\ &\le \lambda_\#^{-(K-1)}\left(\left\|\tau_+^s\right\|+1\right)r.\end{aligned}$$

Note that for the stable free-boundary solution, (24) implies $\bar{x}_k \in E^s$, $k \ge 1$; hence

$$\bar{x}_k^u = 0,$$

which, in turn, implies

$$\|x_K^u - \bar{x}_K^u\| = \|x_K^u\| \le \lambda_\#^{-(K-1)}\left\|\tau_+^s\right\| r.$$

It follows from this that

$$\begin{aligned}\|x_k^u-\bar{x}_k^u\| = \|x_k^u\| &= \left\|F^{-(K-k)}x_K^u\right\| \\ &\le \lambda_\#^{-(K-k)}\|x_K^u\| \le \lambda_\#^{-(K-k)}\lambda_\#^{-(K-1)}\left\|\tau_+^s\right\| r \\ &= \lambda_\#^{-2K+k+1}\left\|\tau_+^s\right\| r.\end{aligned} \tag{A21}$$

On the other hand,

$$\begin{aligned}\|x_1^s-\bar{x}_1^s\| &\le \varepsilon_1(1-\varepsilon_1)^{-1}\left\|F^d x_0\right\|+\varepsilon_2(1-\varepsilon_2)^{-1}\|x_1\| \\ &\le \max\left[\varepsilon_1(1-\varepsilon_1)^{-1},\varepsilon_2(1-\varepsilon_2)^{-1}\right]r \\ &\le 2\max(\varepsilon_1,\varepsilon_2)r \\ &\le 2\lambda_\#^{-2K}\max\left(\alpha_-^{-1},\alpha_+^{-1}\lambda_\#^2\right)r\end{aligned}$$

where (A3) was used. Therefore

$$\begin{aligned}\|x_k^s-\bar{x}_k^s\| &= \left\|F^{k-1}(x_1^s-\bar{x}_1^s)\right\| \\ &\le \lambda_\#^{-(k-1)}\|x_1^s-\bar{x}_1^s\| \\ &\le \lambda_\#^{-(k-1)}2\lambda_\#^{-2K}\max\left(\alpha_-^{-1},\alpha_+^{-1}\lambda_\#^2\right)r \\ &= \lambda_\#^{-2K-k+1}2\max\left(\alpha_-^{-1},\alpha_+^{-1}\lambda_\#^2\right)r.\end{aligned} \tag{A22}$$

It follows from (A21) and (A22) that

$$\begin{aligned}\sum_{k=1}^{K}\|\boldsymbol{x}_k-\bar{\boldsymbol{x}}_k\|^2 &\le \sum_{k=1}^{K}\|\boldsymbol{x}_k^u-\bar{\boldsymbol{x}}_k^u\|^2+\sum_{k=1}^{K}\|\boldsymbol{x}_k^s-\bar{\boldsymbol{x}}_k^s\|^2\\ &\le \sum_{k=1}^{K}\lambda_{\#}^{-4K+2k+2}\|\boldsymbol{\tau}_+^s\|^2r^2\\ &\quad+\sum_{k=1}^{K}\lambda_{\#}^{-4K-2k+2}\\ &\quad\cdot 4\left\{\max\left(\alpha_-^{-1},\alpha_+^{-1}\lambda_{\#}^2\right)\right\}^2r^2\\ &=\left(\sum_{k=1}^{K}\lambda_{\#}^{2k}+\sum_{k=1}^{K}\lambda_{\#}^{-2k}\right)\lambda_{\#}^{-4K+2}r^2\\ &\quad\cdot\max\left(\|\boldsymbol{\tau}_+^s\|^2,4\left\{\max\left(\alpha_-^{-1},\alpha_+^{-1}\lambda_{\#}^2\right)\right\}^2\right)\\ &\quad\to 0\quad\text{as}\quad K\to+\infty.\end{aligned}$$

Using a similar argument, one can show that

$$\sum_{k=-K}^{0}\|\boldsymbol{x}_k-\bar{\boldsymbol{x}}_k\|^2\to 0\quad\text{as}\quad K\to+\infty.\qquad\square$$

Appendix II
Proof of Proposition 6

(i) If μ is an eigenvalue of $\boldsymbol{A}$,

$$\boldsymbol{A}_\mu:=\boldsymbol{A}-\mu\boldsymbol{1}\tag{A23}$$

is singular, and hence it is not negative definite. Therefore $\boldsymbol{A}_\mu$ cannot be temporally stable. If

$$a_0-\mu<0\tag{A24}$$

then Proposition 2 says that $Q_\mu(\omega)$ defined by (45) for $\boldsymbol{A}_\mu$ has a real zero on $(-2,2)$ with odd multiplicity. Since the multiplicity is odd, the zero on $(-2,2)$ cannot be an extremum of Q_μ so that

$$\min_{\omega\in[-2,2]}Q_\mu(\omega)<0\quad\text{and}\quad\max_{\omega\in[-2,2]}Q_\mu(\omega)>0\tag{A25}$$

which is equivalent to

$$\min_{\omega\in[-2,2]}a_mQ_\mu(\omega)<0<\max_{\omega\in[-2,2]}a_mQ_\mu(\omega).\tag{A26}$$

Since

$$a_mQ_\mu(\omega)=a_0-\mu+\sum_{p=1}^{m}a_p\left(\lambda^p+\lambda^{-p}\right)\tag{A27}$$

where ω and λ are related via (44), one has

$$a_mQ_\mu(\omega)=a_mQ(\omega)-\mu.\tag{A28}$$

Equations (A26) and (A28) imply (66). In order to consider the case

$$a_0-\mu>0\tag{A29}$$

one needs the following:

Lemma A2: If $a_0-\mu>0$, the following are equivalent:

i) $\boldsymbol{A}_\mu$ is *positive* definite for all n.

ii) The corresponding spatial dynamics are regular.

iii) Every real zero of Q_μ on $(-2,2)$ has an even multiplicity.

Proof: Recall (49) and replace $-a_p$ by a_p:

$$a_p=\sum_{p=1}^{m-p}z_iz_{i+p},\qquad p=1,\cdots,m$$

$$a_0-\mu=\sum_{p=0}^{m}z_i^2.$$

One can use an argument similar to that used in the proof of Theorem 2 and Proposition 2 to show the result. $\square$

In order to complete the proof of (i) of Proposition 6, observe the fact that $\boldsymbol{A}_\mu$ being singular violates (i)–(iii) in Lemma A2. Since (iii) of Lemma A2 is the same as (iii) of Proposition 2, one can use the same argument as for $a_0-\mu<0$. It is clear from the form of $\boldsymbol{A}$ and $a_0\neq 0$, $a_m\neq 0$ that $a_0-\mu=0$ is impossible.

(ii) In order to prove the optimality of the upper bound, note that for any $\gamma\in\mathbb{R}$

$$\sigma_+(a_0+\gamma,a_1,\cdots,a_m)=\sigma_+(a_0,a_1,\cdots,a_m)+\gamma.\tag{A30}$$

Now fix $a_1,\cdots,a_m$ and consider

$$P_n(a_0-\mu,a_1,\cdots,a_m):=\det(\boldsymbol{A}-\mu\boldsymbol{1})\tag{A31}$$

where n denotes the size of $\boldsymbol{A}$. It follows from (A31) that if $\{\mu_{n,i}(a_0^n)\}_{i=1}$ and $\{\mu_{n,j}(a_0^n)\}_{j=1}$ are the eigenvalues of $\boldsymbol{A}$ when the diagonal is a_0 and a_0', respectively, then by an appropriate relabeling,

$$\mu_{n,i}(a_0)-a_0=\mu_{n,i}(a_0')-a_0',\qquad i=1,\cdots,n.\tag{A32}$$

In order to demonstrate the optimality of the upper bound, we first consider the case

$$\sigma_+(a_0,a_1,\cdots,a_m)=0.$$

If this is not optimal, there is a $\delta>0$ such that

$$\mu_{n,i}(a_0,a_1,\cdots,a_m)<-\delta<\sigma_+(a_0,a_1,\cdots,a_m)\tag{A33}$$

for all n and $1\le i\le n$. It follows from (A32) that

$$\begin{aligned}&\mu_{n,i}(a_0+\delta/2,\ a_1,\cdots,a_m)-(a_0+\delta/2)\\ &\quad=\mu_{n,i}(a_0,a_1,\cdots,a_m)-a_0\end{aligned}$$

whence

$$\mu_{n,i}(a_0,a_1,\cdots,a_m)=\mu_{n,i}(a_0+\delta/2,a_1,\cdots,a_m)-\delta/2\tag{A34}$$

for all n and $1\le i\le n$. Equation (A33) and (A34) imply

$$\mu_{n,i}(a_0+\delta/2,a_1,\cdots,a_m)<-\delta/2<0\tag{A35}$$

for all n and $1\le i\le n$. This means that $(a_0+\delta/2,a_1,\cdots,a_m)$ results in the temporal stability. On the other hand (A30) implies

$$\begin{aligned}\sigma_+(a_0+\delta/2,a_1,\cdots,a_m)&=\sigma_+(a_0,a_1,\cdots,a_m)\\ &\quad+\delta/2=\delta/2>0.\end{aligned}$$

This contradicts (A35) because Proposition 4 says that the temporal stability is equivalent to $\sigma_+<0$. In order to show

the general case

$$\sigma_+(a_0, a_1, \cdots, a_m) = \sigma^*$$

suppose that σ^* is not optimal. Then, there is a $\delta > 0$ such that

$$\mu_{n,i}(a_0, a_1, \cdots, a_m) < \sigma^* - \delta \tag{A36}$$

for all n and $1 \leq i \leq n$. It follows from (A32) that

$$\mu_{n,i}(a_0, a_1, \cdots, a_m) - a_0 = \mu_{n,i}(a_0 - \sigma^*, a_1, \cdots, a_m) - (a_0 - \sigma^*) \tag{A37}$$

for all n and $1 \leq i \leq n$. Equations (A36) and (A37) imply

$$\mu_{n,i}(a_0 - \sigma^*, a_1, \cdots, a_m) < -\delta \tag{A38}$$

for all n and $1 \leq i \leq n$. It follows from (A30) that

$$\sigma_+(a_0 - \sigma^*, a_1, \cdots, a_m) = 0.$$

It was shown earlier than when $\sigma_+ = 0$, it is the optimal upper bound. Therefore, (A38) contradicts the optimality. In order to show the optimality of the lower bound $\sigma_-(a_0, a_1, \cdots, a_m)$, note that

$$\sigma_+(-a_0, -a_1, \cdots, -a_m) = -\sigma_-(a_0, a_1, \cdots, a_m).$$

Furthermore, if μ is an eigenvalue of $\boldsymbol{A}$, then $-\mu$ is an eigenvalue of $-\boldsymbol{A}$. Since $-\sigma_-(a_0, a_1, \cdots, a_m)$ is the optimal upper bound for $-\boldsymbol{A}$, i.e.,

$$-\mu_{n,i}(a_0, a_1, \cdots, a_m) < -\sigma_-(a_0, a_1, \cdots, a_m)$$

one sees that

$$\sigma_-(a_0, a_1, \cdots, a_m) < \mu_{n,i}(a_0, a_1, \cdots, a_m)$$

and σ_- is optimal. □

APPENDIX III
PROOF OF PROPOSITION 7

We will give all the details for the sake of completeness. Since $m = 2$, $\boldsymbol{F}$ is 4×4 and is given by

$$\begin{bmatrix} 0 & 1 & 0 & 0 \\ 0 & 0 & 1 & 0 \\ 0 & 0 & 0 & 1 \\ -1 & -\frac{a_1}{a_2} & -\frac{a_0}{a_2} & -\frac{a_1}{a_2} \end{bmatrix}$$

The characteristic polynomial is

$$P_F(\lambda) = \lambda^2 \left[\frac{a_0}{a_2} + \frac{a_1}{a_2}(\lambda + \lambda^{-1}) + (\lambda^2 + \lambda^{-2}) \right]$$

and

$$Q(\omega) = \omega^2 + \frac{a_1}{a_2}\omega + \frac{a_0}{a_2} - 2 = \left(\omega + \frac{1}{2}\frac{a_1}{a_2}\right)^2 - \frac{1}{4}\left(\frac{a_1}{a_2}\right)^2 + \frac{a_0}{a_2} - 2.$$

Case 1:

$$-\frac{1}{2}\frac{a_1}{a_2} \leq -2.$$

Since

$$\max_{\omega \in [-2,2]} Q(\omega) = Q(2), \qquad \min_{\omega \in [-2,2]} Q(\omega) = Q(-2)$$

one has

$$\sigma_+(a_0, a_1, a_2) = \begin{cases} a_2 Q(2) & \text{when } a_2 > 0 \\ a_2 Q(-2) & \text{when } a_2 < 0 \end{cases}$$

$$\sigma_-(a_0, a_1, a_2) = \begin{cases} a_2 Q(-2) & \text{when } a_2 < 0 \\ a_2 Q(2) & \text{when } a_2 > 0. \end{cases}$$

Case 2:

$$-\frac{1}{2}\frac{a_1}{a_2} \geq 2$$

$$\max_{\omega \in [-2,2]} Q(\omega) = Q(-2), \qquad \min_{\omega \in [-2,2]} Q(\omega) = Q(2)$$

$$\sigma_+(a_0, a_1, a_2) = \begin{cases} a_2 Q(-2) & \text{when } a_2 > 0 \\ a_2 Q(2) & \text{when } a_2 < 0 \end{cases}$$

$$\sigma_-(a_0, a_1, a_2) = \begin{cases} a_2 Q(2) & \text{when } a_2 > 0 \\ a_2 Q(-2) & \text{when } a_2 < 0. \end{cases}$$

Case 3:

$$-2 \leq -\frac{1}{2}\frac{a_1}{a_2} \leq 0$$

$$\max_{\omega \in [-2,2]} Q(\omega) = Q(2), \qquad \min_{\omega \in [-2,2]} Q(\omega) = Q(-a_1/2a_2)$$

$$\sigma_+(a_0, a_1, a_2) = \begin{cases} a_2 Q(2) & \text{when } a_2 > 0 \\ a_2 Q(-a_1/2a_2) & \text{when } a_2 < 0 \end{cases}$$

$$\sigma_-(a_0, a_1, a_2) = \begin{cases} a_2 Q(-a_1/2a_2) & \text{when } a_2 > 0 \\ a_2 Q(2) & \text{when } a_2 < 0. \end{cases}$$

Case 4:

$$0 < -\frac{1}{2}\frac{a_1}{a_2} < 2$$

$$\max_{\omega \in [-2,2]} Q(\omega) = Q(-2), \qquad \min_{\omega \in [-2,2]} Q(\omega) = Q(-a_1/2a_2)$$

$$\sigma_+(a_0, a_1, a_2) = \begin{cases} a_2 Q(-2) & \text{when } a_2 > 0 \\ a_2 Q(-a_1/2a_2) & \text{when } a_2 < 0 \end{cases}$$

$$\sigma_-(a_0, a_1, a_2) = \begin{cases} a_2 Q(-a_1/2a_2) & \text{when } a_2 > 0 \\ a_2 Q(-2) & \text{when } a_2 < 0. \end{cases}$$

Now note that

$$Q(2) = 2 + 2\frac{a_1}{a_2} + \frac{a_0}{a_2} \tag{A39}$$

$$Q(-2) = 2 - 2\frac{a_1}{a_2} + \frac{a_0}{a_2} \tag{A40}$$

$$Q\left(-\frac{1}{2}\frac{a_1}{a_2}\right) = -\frac{1}{4}\left(\frac{a_1}{a_2}\right)^2 + \frac{a_0}{a_2} - 2. \tag{A41}$$

In order to obtain the desired final form, we need to check the following cases:

i) $a_2 > 0$ and *case 1* $\leftrightarrow a_1 \geq 4a_2 > 0$
ii) $a_2 > 0$ and *case 2* $\leftrightarrow a_1 \leq -4a_2 < 0$
iii) $a_2 > 0$ and *case 3* $\leftrightarrow 0 \leq a_1 < 4a_2$
iv) $a_2 > 0$ and *case 4* $\leftrightarrow -4a_2 < a_1 < 0$
v) $a_2 < 0$ and *case 1* $\leftrightarrow a_1 \leq 4a_2 < 0$

vi) $a_2 < 0$ and *case 2* $\leftrightarrow a_1 \geq -4a_2 > 0$
vii) $a_2 < 0$ and *case 3* $\leftrightarrow 4a_2 < a_1 \leq 0$
viii) $a_2 < 0$ and *case 4* $\leftrightarrow -4a_2 > a_1 > 0$.

It follows from (A39)–(A41) that

$$\sigma_+(a_0, a_1, a_2) = \begin{cases} a_2 Q(2) & \text{when (i) or (iii) or (vi)} \\ a_2 Q(-2) & \text{when (ii) or (iv) or (v)} \\ a_2 Q(-a_1/2a_2) & \text{when (vii) or (viii)} \end{cases} \tag{A42}$$

$$\sigma_-(a_0, a_1, a_2) = \begin{cases} a_2 Q(2) & \text{when (ii) or (v) or (vii)} \\ a_2 Q(-2) & \text{when (i) or (iv) or (viii)} \\ a_2 Q(-a_1/2a_2) & \text{when (iii) or (iv).} \end{cases} \tag{A43}$$

It follows from (3) that

$$a_0 = -(g_0 + 2g_1 + 2g_2), \qquad a_1 = g_1, \qquad a_2 = g_2$$

so that (A39)–(A41) give

$$a_2 Q(2) = g_2 \left[2 + 2\frac{g_1}{g_2} - \frac{1}{g_2}(g_0 + 2g_1 + 2g_2) \right] = -g_0 \tag{A44}$$

$$a_2 Q(-2) = g_2 \left[2 + 2\frac{g_1}{g_2} - \frac{1}{g_2}(g_0 + 2g_1 + 2g_2) \right] = -g_0 - 4g_1 \tag{A45}$$

$$a_2 Q\left(-\frac{g_1}{2g_2}\right) = g_2 \left[-\frac{1}{4}\left(\frac{g_1}{g_2}\right)^2 - \frac{1}{g_2}(g_0 + 2g_1 + 2g_2) - 2 \right] = -g_0 - 2g_1 - 4g_2 - g_1^2/4g_2. \tag{A46}$$

Substituting (A44)–(A46) into (A42) and (A43), one has the relations shown at the bottom of the page. It is easy to see that these are the ones given by (67). □

Appendix IV

In [1], $g_0, g_1 > 0$ while $g_2 < 0$, and $g_1 = 4|g_2|$. We will give a simple explanation for the reader who is unfamiliar with the regularization theory [2], [3].

Let a set of noisy data $x_1, \cdots, x_n$ be given. Suppose one wants to interpolate the data with appropriate smoothness. A reasonable way of accomplishing this is to minimize

$$G(v) = \sum_{k=1}^{n} (x_k - v_k)^2 + \lambda \sum_{k=1}^{n} (2v_k - v_{k-1} - v_{k+1})^2 \tag{A47}$$

with respect to $\boldsymbol{v} = (v_1, \cdots, v_n)$. The first term is called the data term while the second term is called the penalty term and it represents the penalty on the "second-order derivative," i.e.,

$$\approx \lambda \int \left(\frac{d^2 v(x)}{dx^2} \right)^2 dx$$

and $\lambda > 0$ is the weight on the penalty. Since this is a straightforward quadratic minimization problem, the solution is obtained by differentiating (A47) with respect to v_k and setting it to zero:

$$x_k - v_k + \lambda[-6v_k + 4(v_{k-1} + v_{k+1}) - (v_{k-2} + v_{k-2})] = 0$$

and hence

$$-(1/\lambda + 6)v_k + 4(v_{k-1} + v_{k+1}) - (v_{k-2} + v_{k+2}) + (1/\lambda)x_k = 0. \tag{A48}$$

If $g_0, g_1 > 0$, $g_2 < 0$, and $g_1/|g_2| = 4$, $g_0/|g_2| = 1/\lambda$, then (A48) reads

$$-(g_0 + 2g_1 + 2g_2)v_k + g_1(v_{k-1} + v_{k+1}) + g_2(v_{k-2} + v_{k+2}) + u_k = 0$$

which is exactly (8) with $m = 2$, where $u_k = (1/\lambda)x_k$. Thus, by varying g_0 while g_1 and g_2 are fixed, one can control the weight λ which corresponds to varying the width of the Gaussian-like kernel. It should be noticed, however, that the architecture shown in Fig. 1 is a rather crude approximation for the two-dimensional problem.

Conversely, given a circuit, one can recover $G(\boldsymbol{v})$ as the *total cocontent:*

$$G(v) = \frac{1}{2}\boldsymbol{v}^T \boldsymbol{A}\boldsymbol{v} + \boldsymbol{v}^T \boldsymbol{u}$$

and the dynamics of the circuit minimizes $-G(\boldsymbol{v})$ by

$$\frac{d}{dt}[-G(\boldsymbol{v}(t))] = -(\boldsymbol{A}\boldsymbol{v} + \boldsymbol{u})^T \frac{d\boldsymbol{v}(t)}{dt} = -\frac{d\boldsymbol{v}(t)}{dt}^T \boldsymbol{B}^{-1} \frac{d\boldsymbol{v}(t)}{dt} < 0.$$

Note, however, that if $\boldsymbol{A}$ were not symmetric, the total cocontent would be undefined even if the circuit were linear.

Appendix V
Proof of Proposition 10

Recall D defined by (75).

$$\sigma_+(g_0, g_1, g_2) = \begin{cases} -g_0 & \text{when } g_1, g_2 > 0 \quad \text{or} \quad g_1 > 0, g_2 < 0, |g_1/g_2| \geq 4 \\ -g_0 - 4g_1 & \text{when } g_1 < 0, g_2 > 0 \quad \text{or} \quad g_1 < 0, g_2 < 0, |g_1/g_2| \geq 4 \\ -g_0 - 2g_1 - 4g_2 - g_1^2/4g_2 & \text{when } g_2 < 0, |g_1/g_2| \leq 4 \end{cases}$$

$$\sigma_-(g_0, g_1, g_2) = \begin{cases} -g_0 & \text{when } g_1 < 0, g_2 < 0 \quad \text{or} \quad g_1 < 0, g_2 > 0, |g_1/g_2| \geq 4 \\ -g_0 - 4g_1 & \text{when } g_1 > 0, g_2 < 0 \quad \text{or} \quad g_1 > 0, g_2 > 0, |g_1/g_2| \geq 4 \\ -g_0 - 2g_1 - 4g_2 - g_1^2/4g_2 & \text{when } g_2 > 0, |g_1/g_2| \leq 4. \end{cases}$$

Case 1: $D < 0$. It follows from (72) and (74) that $d\theta/d\omega$ has no real zero and hence Q is monotonically increasing. Therefore

$$\sigma_+ = \begin{cases} a_3 Q(2) & \text{when } a_3 > 0 \\ a_3 Q(-2) & \text{when } a_3 < 0 \end{cases} \tag{A49}$$

$$\sigma_- = \begin{cases} a_3 Q(-2) & \text{when } a_3 > 0 \\ a_3 Q(2) & \text{when } a_3 < 0. \end{cases} \tag{A50}$$

Case 2: $D = 0$. In this case $d\theta/d\omega$ has a double zero. But since Q is cubic, it is monotonically increasing and (A49) and (A50) are true.

Case 3: $D > 0$. This means that $d\theta/d\omega$ has two distinct real zeroes and hence Q has a local maximum at ξ_- and a local minimum at $\xi_+, \xi_- < \xi_+$.

a) $\xi_- < \xi_+ \leq -2$: It is clear that Q is monotonically increasing on $[-2, 2]$ and hence (A49) and (A50) still hold.

b) $2 \leq \xi_- < \xi_+$: Q is monotonically increasing on $[-2, 2]$ and (A49) as well as (A50) is true.

c) $\xi_- \leq -2, 2 \leq \xi_+$: Q is monotonically decreasing on $[-2, 2]$ and

$$\sigma_+ = \begin{cases} a_3 Q(-2) & \text{when } a_3 > 0 \\ a_3 Q(2) & \text{when } a_3 < 0 \end{cases} \tag{A51}$$

$$\sigma_- = \begin{cases} a_3 Q(2) & \text{when } a_3 > 0 \\ a_3 Q(-2) & \text{when } a_3 < 0. \end{cases} \tag{A52}$$

d) $\xi_- \leq -2 \leq \xi_+ \leq 2$: In this case, Q has a local minimum at ξ_+ and hence

$$\sigma_+ = \begin{cases} a_3 \max[Q(-2), Q(2)] & \text{when } a_3 > 0 \\ a_3 Q(\xi_+) & \text{when } a_3 < 0 \end{cases}$$

$$\sigma_- = \begin{cases} a_3 Q(\xi_+) & \text{when } a_3 > 0 \\ a_3 \max[Q(-2), Q(2)] & \text{when } a_3 < 0. \end{cases}$$

e) $-2 \leq \xi_- \leq 2 \leq \xi_+$ Since Q has a local maximum at ξ_-,

$$\sigma_+ = \begin{cases} a_3 Q(\xi_-) & \text{when } a_3 > 0 \\ a_3 \min[Q(-2), Q(2)] & \text{when } a_3 < 0 \end{cases}$$

$$\sigma_- = \begin{cases} a_3 \min[Q(-2), Q(2)] & \text{when } a_3 > 0 \\ a_3 Q(\xi_-) & \text{when } a_3 < 0. \end{cases}$$

f) $-2 \leq \xi_- < \xi_+ \leq 2$: Since Q has a local minimum as well as a local maximum within $[-2, 2]$,

$$\sigma_+ = \begin{cases} a_3 \max[Q(\xi_-), Q(2)] & \text{when } a_3 > 0 \\ a_3 \min[Q(-2), Q(\xi_+)] & \text{when } a_3 < 0 \end{cases}$$

$$\sigma_- = \begin{cases} a_3 \min[Q(-2), Q(\xi_+)] & \text{when } a_3 > 0 \\ a_3 \max[Q(\xi_-), Q(2)] & \text{when } a_3 < 0. \end{cases}$$

Combining all these cases, one obtains the relations given at the bottom of the page, where $f_\pm$ and $h_\pm$ are defined by (77)–(79). □

Appendix VI
Proof of Corollary 1

One can show that the *right derivative*,

$$D^+\|\boldsymbol{v}(t)\| = \lim_{\substack{h \to 0 \\ h > 0}} \frac{\|\boldsymbol{v}(t) + h\dot{\boldsymbol{v}}(t)\| - \|\boldsymbol{v}(t)\|}{h}$$

$$= \left(\lim_{\substack{h \to 0 \\ h > 0}} \frac{\|\boldsymbol{v}(t+h)\| - \|\boldsymbol{v}(t)\|}{h} \right)$$

$$\sigma_+(g_0, g_1, g_2, g_3) = \begin{cases} f_+ & \text{when } g_3 > 0 \text{ and (case 1 or case 2 or case 3-a or case 3-b)} \\ & \text{or } g_3 < 0 \text{ and case 3-c} \\ f_- & \text{when } g_3 < 0 \text{ and (case 1 or case 2 or case 3-a or case 3-b)} \\ & \text{or } g_3 > 0 \text{ and case 3-c} \\ \max[f_+, f_-] & \text{when } g_3 > 0 \text{ and case 3-d} \\ & \text{or } g_3 < 0 \text{ and case 3-e} \\ h_+ & \text{when } g_3 < 0 \text{ and case 3-d} \\ h_- & \text{when } g_3 > 0 \text{ and case 3-e} \\ \max[f_+, h_-] & \text{when } g_3 > 0 \text{ and case 3-f} \\ \max[f_-, h_+] & \text{when } g_3 < 0 \text{ and case 3-f} \end{cases}$$

$$\sigma_-(g_0, g_1, g_2, g_3) = \begin{cases} f_+ & \text{when } g_3 > 0 \text{ and case 3-c} \\ & \text{or } g_3 < 0 \text{ and (case 1 or case 2 or case 3-a or case 3-b)} \\ f_- & \text{when } g_3 < 0 \text{ and case 3-c} \\ & \text{or } g_3 > 0 \text{ and (case 1 or case 2 or case 3-a or case 3-b)} \\ \min[f_+, f_-] & \text{when } g_3 > 0 \text{ and case 3-d} \\ & \text{or } g_3 < 0 \text{ and case 3-e} \\ h_+ & \text{when } g_3 > 0 \text{ and case 3-d} \\ h_- & \text{when } g_3 < 0 \text{ and case 3-e} \\ \min[f_+, h_-] & \text{when } g_3 < 0 \text{ and case 3-f} \\ \min[f_-, h_+] & \text{when } g_3 > 0 \text{ and case 3-f} \end{cases}$$

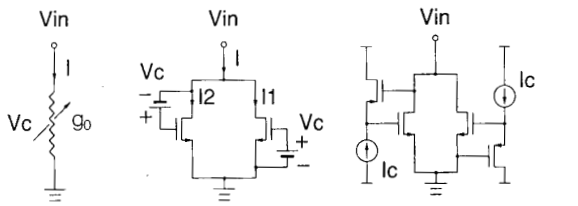

I1 = K[(Vc - Vt) Vin - $\frac{1}{2}$Vin^2] (in triode region)

I2 = K [(Vc + Vin - Vt) Vin - $\frac{1}{2}$ Vin^2]

I = I1 + I2 = 2 K [Vc - Vt] Vin

I = go Vin
where go = 2K [Vc - Vt]

(a)

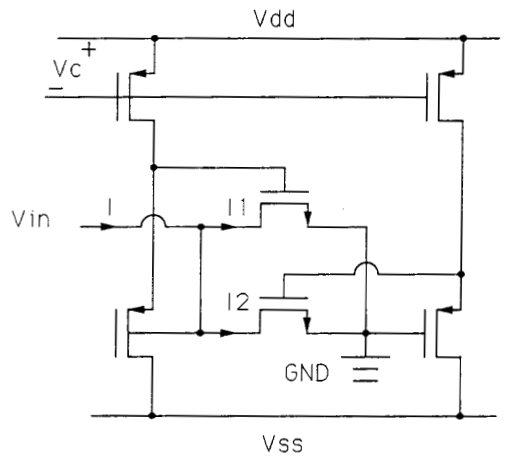

(b)

Fig. 14. Variable conductance g_0. (a) v_c controls the value of g_0. (b) Actual implementation.

exists despite the fact that $\|\boldsymbol{v}(t)\|$ it is *not* differentiable. Since

$$\frac{d\boldsymbol{v}(t)}{dt} = \boldsymbol{B}^{-1}\boldsymbol{A}\boldsymbol{v}(t) + \boldsymbol{B}^{-1}\boldsymbol{u}$$

and since

$$\begin{aligned}&\left\|\boldsymbol{v}(t) + h\boldsymbol{B}^{-1}\boldsymbol{A}\boldsymbol{v}(t) + h\boldsymbol{B}^{-1}\boldsymbol{u}\right\| \\ &\le \left\|\boldsymbol{1} + h\boldsymbol{B}^{-1}\boldsymbol{A}\right\|\|\boldsymbol{v}(t)\| + h\left\|\boldsymbol{B}^{-1}\boldsymbol{u}\right\|\end{aligned}$$

one has

$$\begin{aligned}D^+\|\boldsymbol{v}(t)\| = \lim_{\substack{h\to 0\\ h=0}} \left(\frac{\left\|\boldsymbol{1} + h\boldsymbol{B}^{-1}\boldsymbol{A}\right\| - 1}{h}\right)\|\boldsymbol{v}(t)\| \\ + \left\|\boldsymbol{B}^{-1}\boldsymbol{u}\right\| \qquad \text{(A53)}\end{aligned}$$

where the matrix norm is induced by the Euclidian norm:

$$\left\|\boldsymbol{1} + h\boldsymbol{B}^{-1}\boldsymbol{A}\right\| = \max_{\|\boldsymbol{v}=1\|} \left\|\left(\boldsymbol{1} + h\boldsymbol{B}^{-1}\boldsymbol{A}\right)\boldsymbol{v}\right\|.$$

One can easily show that the right-hand limit of the first term in (A53) also exists. Denoting this limit by

$$m\left(\boldsymbol{B}^{-1}\boldsymbol{A}\right) := \lim_{\substack{h\to 0\\ h>0}} \frac{\left\|\boldsymbol{1} + h\boldsymbol{B}^{-1}\boldsymbol{A}\right\| - 1}{h}$$

one has the right *differential inequality:*

$$\begin{aligned}D^+\|\boldsymbol{v}(t)\| \le m\left(\boldsymbol{B}^{-1}\boldsymbol{A}\right)\|\boldsymbol{v}(t)\| + \left\|\boldsymbol{B}^{-1}\boldsymbol{u}\right\|, \\ \|\boldsymbol{v}(0)\| = 0.\end{aligned}$$

It is not difficult to show that a solution of a differential inequality is bounded by the solution of the corresponding differential equation:

$$\begin{aligned}\frac{dw}{dt} = m\left(\boldsymbol{B}^{-1}\boldsymbol{A}\right)w + \left\|\boldsymbol{B}^{-1}\boldsymbol{u}\right\|, \\ w(0) = 0.\end{aligned}$$

Therefore

$$\|\boldsymbol{v}(t)\| \le \frac{1}{m\left(\boldsymbol{B}^{-1}\boldsymbol{A}\right)}\left[\exp\left(m\left(\boldsymbol{B}^{-1}\boldsymbol{A}\right)t - 1\right)\right]\left\|\boldsymbol{B}^{-1}\boldsymbol{u}\right\|. \qquad \text{(A54)}$$

Similarly, the *left derivative* satisfies

$$\begin{aligned}D^-\|\boldsymbol{v}(t)\| &\ge \lim_{\substack{h\to 0\\ h<0}} \left(\frac{\left\|\boldsymbol{1} + h\boldsymbol{B}^{-1}\boldsymbol{A}\right\| - 1}{h}\right)\|\boldsymbol{v}(t)\| \\ &\quad + \left\|\boldsymbol{B}^{-1}\boldsymbol{u}\right\| \\ &= -m\left(\boldsymbol{B}^{-1}\boldsymbol{A}\right)\|\boldsymbol{v}(t)\| + \left\|\boldsymbol{B}^{-1}\boldsymbol{u}\right\|,\end{aligned}$$

$$\|\boldsymbol{v}(0)\| = 0,$$

which yields

$$\begin{aligned}\|\boldsymbol{v}(t)\| \ge \frac{1}{-m\left(-\boldsymbol{B}^{-1}\boldsymbol{A}\right)} \\ \cdot \left[\exp\left(-m\left(-\boldsymbol{B}^{-1}\boldsymbol{A}\right)t\right) - 1\right]\left\|\boldsymbol{B}^{-1}\boldsymbol{u}\right\|. \qquad \text{(A55)}\end{aligned}$$

Finally, it is known [24] that

$$m\left(\boldsymbol{B}^{-1}\boldsymbol{A}\right) = \text{max. eigenvalue of } \boldsymbol{B}^{-1}\boldsymbol{A} \qquad \text{(A56)}$$

and hence

$$-m\left(-\boldsymbol{B}^{-1}\boldsymbol{A}\right) = \text{min. eigenvalue of } \boldsymbol{B}^{-1}\boldsymbol{A}. \qquad \text{(A57)}$$

It follows from (66), (84), and (A56) that

$$m\left(\boldsymbol{B}^{-1}\boldsymbol{A}\right) \le \frac{\sigma_+}{\eta_+}. \qquad \text{(A58)}$$

Similarly

$$-m\left(-\boldsymbol{B}^{-1}\boldsymbol{A}\right) \ge \frac{\sigma_-}{\eta_-}. \qquad \text{(A59)}$$

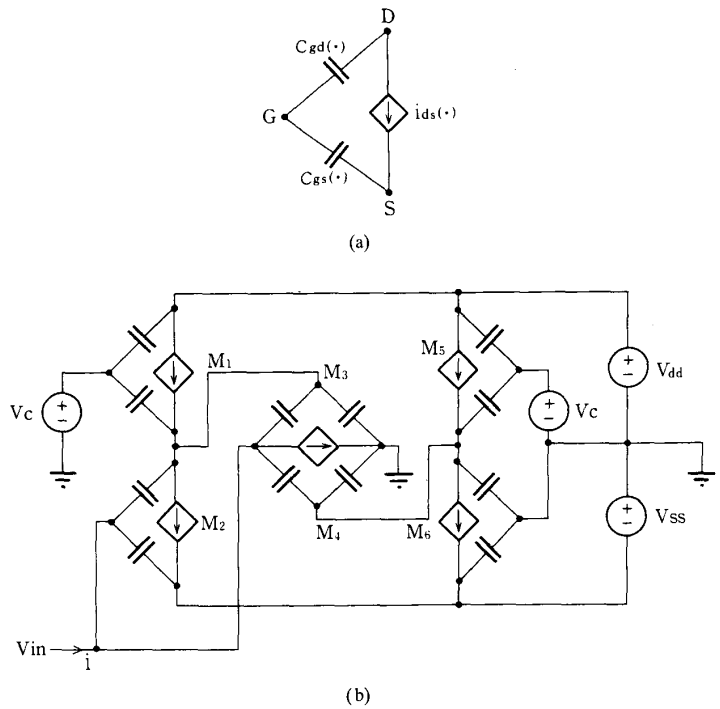

Fig. 15. Equivalent circuit of the g_0 circuit. (a) Equivalent circuit of an NMOS transistor; $i_{ds}(\cdot)$ indicates that the controlled current source is nonlinear, and $c_{gs}(\cdot)$ and $c_{gd}(\cdot)$ stand for nonlinear capacitors. (b) Equivalent circuit of Fig. 14(b).

Substituting (A58) and (A59) into (A54) and (A55), one has the desired bounds. □

APPENDIX VII

This appendix tries to justify the model given by (1)–(4). There are two aspects that must be examined:

i) resistive part $g_0, g_1, \cdots, g_m$;
ii) capacitive part $c_0, c_1, \cdots, c_m$.

Although these parameters are implementation dependent, we can give a fairly reasonable account of them by checking the Gaussian-like convolver chip [1], where $m = 2$. Let us first look at Fig. 14, which implements g_0. Fig. 14(a) shows how g_0 can be made variable by controlling v_c, while Fig. 14(b) shows the actual implementation. In order to examine how this circuitry affects the resistive as well as the capacitive part of the model, one naturally has to have an equivalent circuit of each transistor. While a resistive part of an MOS transistor can be described by a simple nonlinear model, the capacitive part is known to be difficult to model [25]. In some cases it is described as a nonlinear distributed parameter element [26], and in some other cases it is described as a nonlinear, nonreciprocal multiterminal capacitor [27]. In many practical situations, parasitic capacitors are reciprocal and each is regarded as constant in each of the operating regions (cutoff, triode, and saturation) [25], [28], although they are still nonlinear, i.e., piecewise constant. (One has to be careful about the charge conservation because the incremental capacitance is discontinuous.) In many cases, a zero bulk charge is assumed. Fig. 15(a) gives such an equivalent circuit, where $i_{ds}(\cdot)$ indicates that the (controlled) current source is nonlinear, and $c_{gs}(\cdot)$ (resp. $c_{gd}(\cdot)$) represents nonlinear gate–source (resp. gate–drain) capacitor. A similar circuit can be given for a PMOS. Fig. 15(b) shows an equivalent circuit of Fig. 14(b) using Fig. 15(a). In order to examine the resistive part of the circuit, open-circuit all the capacitors. Fig. 16(a) shows the SPICE-simulated v_{in}–i characteristics while Fig. 16(b) gives measured characteristics which verify that the resistive part behaves in a sufficiently linear manner within the operating range. It should be noted that no small-signal argument is used. Namely, the linearity of the v_{in}–i characteristics does not mean that each transistor operates linearly. In fact, the four PMOS transistors are designed to operate in the saturation region.

Next let us look at Fig. 17(a), which implements g_2, where $R_2 > 0$ is a p-well resistor and the remaining circuit realizes a negative impedance converter, where a triangle stands for a standard transconductance amplifier. Parts (b) and (c) of Fig. 17 give SPICE simulated and measured characteristics, respectively. In [1], g_1 is realized by a p-well resistor. Fig. 18 shows a SPICE simulation of a spatial impulse response at the *transistor* level. The reader is referred to [1] for measured impulse responses.

The capacitive part of the circuit needs more care to examine. In order to evaluate c_0, let us first check the g_0 circuit. To this end, open-circuit the current sources and short-circuit the voltage sources of Fig. 15(b) and obtain Fig. 19(a).

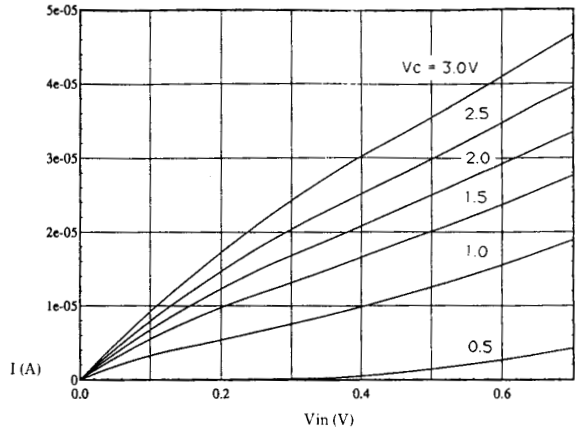

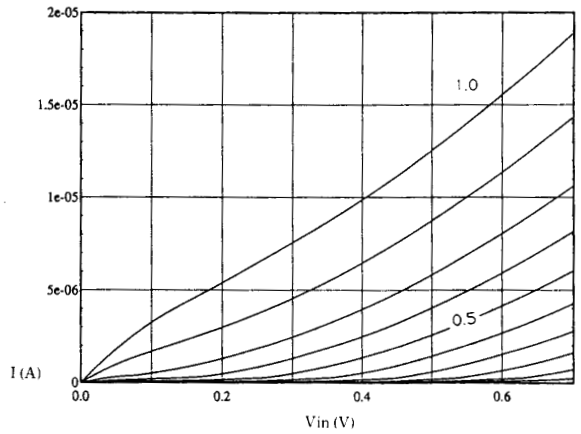

(a)

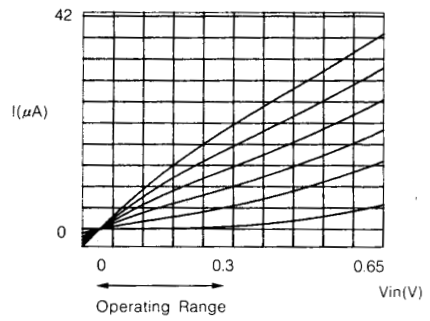

(b)

Fig. 16. The $v_{\text{in}} - i$ characteristics of Fig. 14(b). (a) SPICE simulated. (b) Measured.

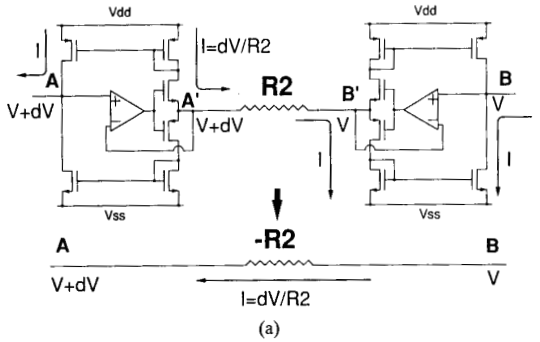

(a)

——— Actual Negative Resistor

— — — Ideal Negative Resistor

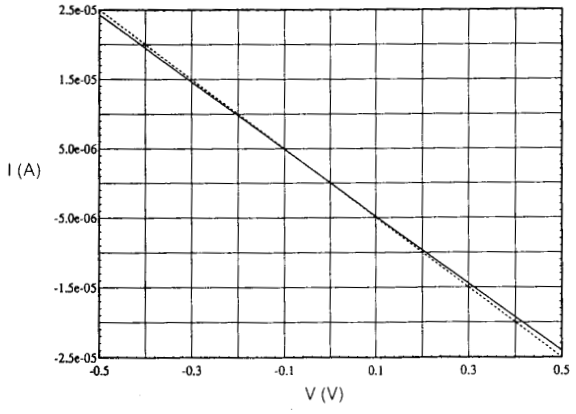

(b)

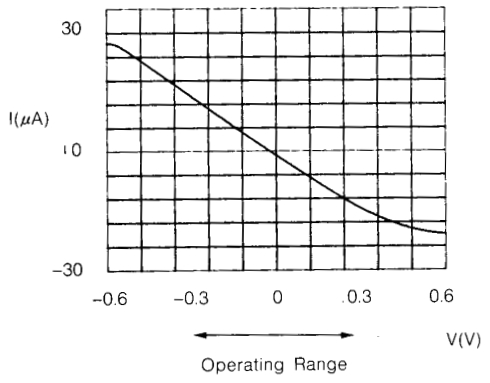

(c)

Fig. 17. Negative conductance g_2. (a) Circuitry. (b) SPICE simulated. (c) Measured.

That the resistive part behaves linearly does *not* guarantee that the capacitive part also behaves linearly. However, the pair of NMOS's in the middle is designed to operate in the triode region while the rest is designed to operate in the saturation region. Since we are assuming that each capacitance is constant in each operating region, c_{gd}'s and c_{gs}'s can be regarded as constant so that one can compute the overall equivalent capacitance, say c_0', between the v_{in} terminal and the ground. Since Fig. 19(a) is reduced to Fig. 19(b), one has

$$c_0' = \frac{(c_{02} + c_{04})(c_{01} + c_{05})}{c_{01} + c_{02} + c_{04} + c_{05}} + \frac{c_{06}(c_{07} + c_{08} + c_{09})}{c_{06} + c_{07} + c_{08} + c_{09}} + c_{03} \tag{A60}$$

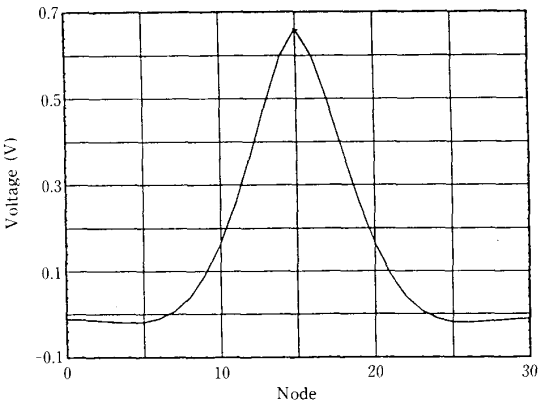

Fig. 18. SPICE simulated spatial impulse response at the transistor level where $1/g_1$ and $1/g_2$ are intended for 5 kΩ and −20 kΩ, respectively.

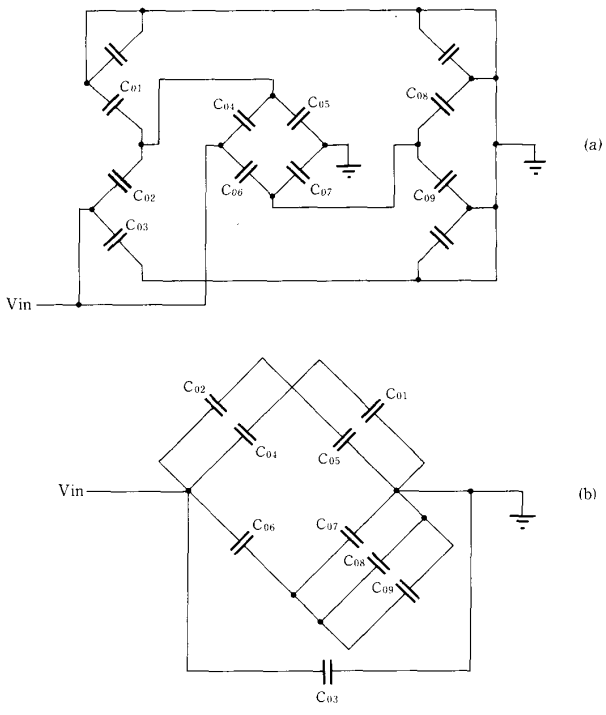

Fig. 19. Capacitive part of Fig. 15(b). (a) Original circuit. (b) Equivalent circuit.

Despite the fact that there are as many as nine capacitors contributing to c_0', the actual c_0' value would be very small. This stems from the fact that in the triode region, $c_{gs} = c_{gd} \approx (1/2)WLc_{ox}$ while in the saturation region $c_{gs} \approx (2/3)WLc_{ox}$, $c_{gd} \approx 0$ [25], [28], where W, L, and c_{ox} stand for the channel width, the channel length, and the capacitance (per unit area) of the oxide layer separating the gate from the channel. In this particular implementation, $W/L = 3/8$ (μm) for M_1 and M_5, $4/3$ for M_2 and M_4, and $7/2$ for M_2 and M_6, and $c_{ox} \approx 12 \times 10^{-4}$ pF/μm^2 in the present process. Since g_1 is a p-well resistor, its substrate is connected to v_{dd}. Thus there is a (distributed) diffusion capacitance between each node to v_{dd} (not between two nodes). In discussing the capacitive part of a circuit, one short-circuits voltage source as was done in the g_0 circuit. Therefore, this diffusion capacitance, say c_0'', contributes to c_0. The value of c_0'' would be larger than c_0' because (a) the area of the g_1 in this particular implementation is larger (36×20 μm^2) and (b) diffusion capacitance is the sum of a term proportional to the area and a term proportional to the peripheral length [28].

As for the contribution to c_0 from the g_2 circuit, there are two factors: (a) the parasitic capacitors of MOS transistors and (b) the p-well diffusion capacitance of $R_2 > 0$ (see Fig. 17(a)). The former can be calculated by using the same argument as the one used to compute c_0', while the latter can be estimated using the argument used to discuss the g_1 diffusion capacitance c_0''. If we call the resulting composite capacitance c_0''', the total capacitance between each node and the ground would be $c_0 = c_0' + c_0'' + c_0'''$.

Since conductance g_1 is implemented by a p-well, c_1 naturally represents associated parasitic capacitance between each node to its immediate neighbor. It should be noted, however, that c_1 appears in off-diagonal elements of $\boldsymbol{B}$.

Finally, using the same argument, one can compute the composite capacitance c_2 from each node to its second nearest neighbor. The parasitic capacitor c_2 also appears in off-diagonal elements of $\boldsymbol{B}$.

It follows from (56) that $\boldsymbol{B}$ satisfies the diagonal dominance so that all eigenvalues are (strictly) positive. Naturally, in an actual implementation, $\boldsymbol{B}$ cannot be exactly symmetric. However, eigenvalues being strictly positive is an "open" condition, i.e., small variations of parameters do not destroy the property. We will leave quantitative estimates of those parasitic capacitances for a future paper. We will simply remark that $c_0 = 0.1$ pF used in Fig. 4 would not be too unrealistic.

Fig. 20 shows a simulation result at the *transistor* level on SPICE where $1/g_0$, $1/g_1$, and $1/g_2$ are intended to be 200 kΩ, 5 kΩ, and −20 kΩ, respectively. A subnetwork of 8×8 is simulated (on a Cray) where a step current of duration 5 μs is injected into the four nodes as indicated in Fig. 20(a). Fig. 20(b) shows the voltage responses of the eight nodes on the fourth row. Although the above arguments are far from being complete, we believe that our model is sufficient for the present purpose.

ACKNOWLEDGMENT

The authors greatly appreciate the stimulating discussions with A. A. Abidi and J. L. White of UCLA. Thanks are also due to H. Kokubu of Kyoto University, H. Oka of Ryukoku University, M. W. Hirsch of U. C. Berkeley, M. Kando of the Science University of Tokyo, and A. Hio, K. Tanaka and Y. Takaku of Waseda University for discussions. The reviewers' comments were also very helpful. A part of this work was done while the second author was at UCLA.

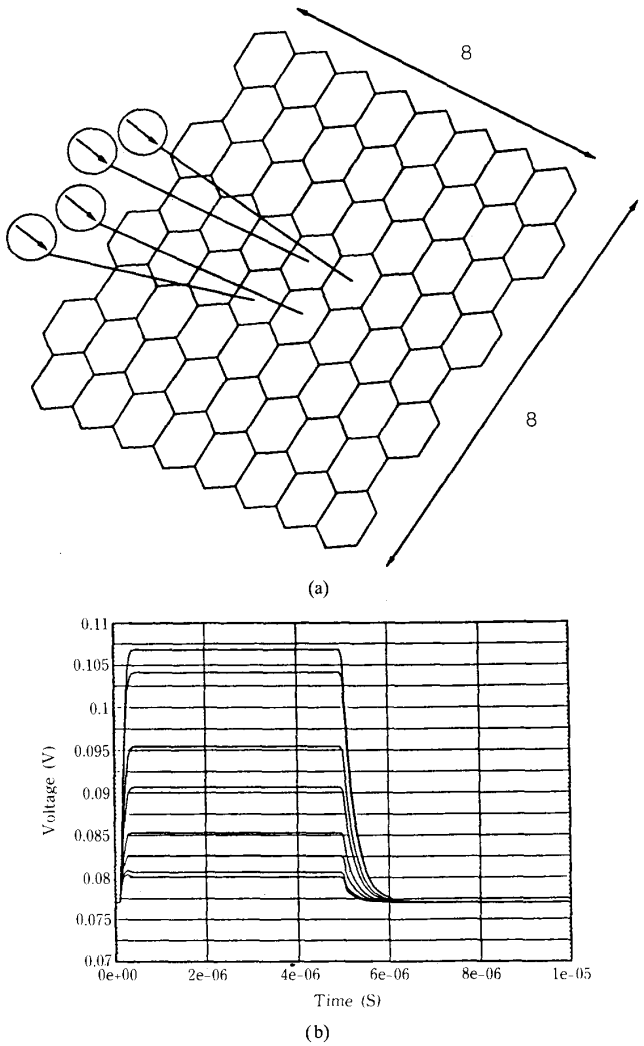

Fig. 20. SPICE simulated temporal step responses at the transistor level. (a) 8 × 8 array is simulated where step current of duration 5 μs is injected to the four nodes as indicated. (b) Voltage responses at the eight nodes in the fourth row.

REFERENCES

[1] H. Kobayashi, J. L. White, and A. A. Abidi, "An active resistor network for Guassian filtering of images," *IEEE J. Solid-State Circuits,* vol. 26, pp. 738–748, May 1991.

[2] T. Poggio, H. Voohees, and A. Yuille, "A regularized solution to edge detection," AI Memo, MIT, Cambridge, MA, May 1985.

[3] T. Poggio, V. Torre, and C. Koch, "Computational vision and regularization theory," *Nature,* vol. 317, pp. 314–319, Sept. 1985.

[4] S. Grossberg, *Adaptive Brain (II).* Amsterdam: North Holland, 1987.

[5] J. G. Dougman, "Image analysis and compact coding by oriented 2D Gabor primitives," *SPIE,* vol. 758, pp. 19–30, 1987.

[6] D. L. Standley and J. L. Wyatt, Jr., "Stability criterion for lateral inhibition and related networks that is robust in the presence of integrated circuit parasitics," *IEEE Trans. Circuits Syst.,* vol. 36, pp. 675–681, May 1989.

[7] C. Mead, *Analog VLSI and Neural Systems.* Reading, MA: Addison-Wesley, 1989.

[8] C. Mead and M. Mahowald, "A silicon model of early visual processing," *Neural Networks,* vol. 1, no. 1, pp. 91–97, 1988.

[9] J. Harris, "An analog VLSI chip for thin-plate surface interpolation," presented at *IEEE Conf. Neural Info. Proc. Systems—Natural and Synthetic,* 1988.

[10] J. Hutchinson, C. Koch, J. Luo, and C. Mead, "Computing motion using analog and binary resistive network," *IEEE Computer,* vol. 21, pp. 52–63, Mar. 1988.

[11] J. Harris, C. Koch, J. Luo, and J. Wyatt, Jr., "Resistive fuses: Analog hardware for detecting discontinuities in early vision," in *Analog VLSI Implementation of Neural Systems.* Norwell, MA: Kluwer Academic, 1989.

[12] A. Lumsdaine, J. Wyatt, and I. Elfadel, "Nonlinear analog networks for image smoothing and segmentation," in *Proc. IEEE ISCAS,* 1990, pp. 987–991.

[13] S. C. Liu and J. Harris, "Generalized smoothing networks in early vision," in *Proc. IEEE Conf. Computer Vision and Pattern Recognition,* 1989, pp. 184–191.

[14] B. Mathur, S. C. Liu, and H. T. Wang, "Analog neural networks for focal-plane image processing," *SPIE,* vol. 1242, pp. 141–151, 1990.

[15] T. Poggio and C. Koch, "Ill-posed problems in early vision: From computation theory to analog networks," *Proc. Roy. Soc. London, Ser. B226,* pp. 303–323, 1985.

[16] M. W. Hirsch and S. Smale, *Differential Equations, Dynamical Systems and Linear Algebra.* New York: Academic, 1974.

[17] T. Kamoto, Y. Akazawa, and M. Shinagawa, "An 8-bit 2-ns monolithic

DAC," *IEEE J. Solid-State Circuits,* vol. 23, no. 1, pp. 142–146, 1988.
[18] E. L. Allgower, "Criteria for positive definiteness of some band matrices," *Numer. Math.,* vol. 16, pp. 157–162, 1970.
[19] F. R. Gantmacher, *The Theory of Matrices.* New York: Chelsea, 1960.
[20] Y. Togawa and T. Matsumoto, "On the topological testability conjecture for analogue fault diagnosis problems," *IEEE Trans. Circuits Syst.,* vol. 31, pp. 147–158, Feb. 1984.
[21] A. V. Oppenheim and R. W. Schafer, *Digital Signal Processing.* Englewood Cliffs, NJ: Prentice Hall, 1975.
[22] J. Moody, "Dynamics of lateral interaction networks," in *Proc. 1990 IJCNN,* vol. III, 1990, pp. 483–486.
[23] S. Amari, "Dynamical study of formation of cortical maps," in *Dynamic Interactions in Neural Networks I,* M. Arbib and S. Amari Eds. New York: Springer, 1989, pp. 15–34.
[24] W. A. Coppel, *Stability and Asymptotic Behavior of Differential Equations.* Boston, MA: Heath, 1965.
[25] L. A. Glasser and R. W. Dobberpuhl, *The Design and Analysis of VLSI Circuits.* Reading, MA: Addison-Wesley, 1985.
[26] J. J. Paulos and D. A. Antoniadis, "Limitations of quasi-static capacitance models for the MOS transistors," *IEEE Electron Devices Lett.,* vol. EDL-4, pp. 221–224, July 1983.
[27] D. E. Ward and R. W. Dutton, "Charge-oriented model for MOS transistor capacitors," *IEEE J. Solid-State Circuits,* vol. SC-13, pp. 703–708, Oct. 1978.
[28] N. Weste and K. Eshraghian, *Principles of CMOS VLSI Design.* Reading, MA: Addison-Wesley, 1985.

Takashi Matsumoto (M'71–SM'83–F'85) was born in Tokyo, Japan, on March 30, 1944. He received the B.Eng. degree in electrical engineering from Waseda University, Tokyo, Japan, the M.S. degree in applied mathematics from Harvard University, Cambridge, MA, and the Dr.Eng. degree in electrical engineering from Waseda University in 1966, 1970, and 1973, respectively.

At present he is Professor of Electrical Engineering, at Waseda University. From 1977 to 1979 he was on leave with the Department of Electrical Engineering and Computer Sciences, University of California at Berkeley. His research interests include nonlinear networks and neural networks.

Within the IEEE, he served as Associate Editor of the TRANSACTIONS ON CIRCUITS AND SYSTEMS and is a member of the Board of Governors of the Circuits and Systems Society. . He was a Guest Editor for the TRANSACTIONS ON CIRCUITS AND SYSTEMS (July 1988) and the PROCEEDINGS OF THE IEEE (August 1987). He is a member of the Circuits and Systems Society's Nonlinear Circuits and Systems Technical Committee and Neural Networks Technical Committee. He serves on the editorial board of the PROCEEEDINGS OF THE IEEE and is Vice Chairperson of the Tokyo Chapter of the Circuits and Systems Society.

Dr. Matsumoto is a member of the Institute of Electronics, Information and Communication Engineering (the IEICE—Japan's counterpart to the IEEE). He was chairperson of the Nonlinear Problems Technical Committee and was on the editorial boards of the *Transactions of the IEICE* and the *Journal of the IEICE.*

In addition, he serves on the editorial board of the journal *Circuits, Systems and Signal Processing* (Elsevier).

Haruo Kobayashi (S'88–M'90) was born in Utsunomiya, Japan, in 1958. He received the B.S. and M.S. degrees in information physics and mathematical engineering from the University of Tokyo in 1980 and 1982 respectively. From 1987 to 1989, he was at the University of California, Los Angeles, where he received the M.S. degree in electrical engineering in 1989.

He joined Yokogawa Electric Corporation, Tokyo, Japan, in 1982, where he has been engaged in research and development work on an FFT analyzer, a mini-supercomputer, and an LSI tester. His recent research interests include analog CMOS IC design and neural networks.

Mr. Kobayashi is a member of the Institute of Electronics, Information and Communication Engineers of Japan and the Society of Instrument and Control Engineers of Japan.

Yoshio Togawa was born in Tokyo, Japan, on January 5, 1953. He received the B.Sc., M.Sc., and Dr.Sc. degrees in mathematics from Waseda University, Tokyo, Japan, in 1975, 1977, and 1981, respectively.

Since 1977, he has been with the Science University of Tokyo, where his research has dealt mainly with dynamical systems.